Cr^{III} as an alternative to Ru^{II} in metallo-supramolecular chemistry

Davood Zare, Benjamin Doistau,* Homayoun Nozary, Céline Besnard, Laure Guénée, Yan Suffren, Anne-Laure Pelé, Andreas Hauser* and Claude Piguet*

Supporting Information

(85 pages)

Table S1 Elemental analyses found for $[M(tpy)_2](PF_6)_3$ (M = Ga, Cr), $[Cr(ebzpy)_2](PF_6)_3$, $[Cr(L)Cl_3]$ (L = tpy, ebzpy, tppz, ddpd), $[Cr(L)(CF_3SO_3)_3]$ (L = tpy, tppz), $[Cr(tpy)(ebzpy)](PF_6)_3$, $[Cr(tpy)(tppz)](CF_3SO_3)_3$, $[Cr_2Cl_6(L)]$ and $[Cr_2(tpy)_2(L)](PF_6)_6$ (L = ttpz, bbt, ebbt).[a]

Compound	MM/ $g \cdot mol^{-1}$	%C found	%H found	%N found	%C Calcd.	%H Calcd	%N Calcd.
$[Ga(tpy)_2](PF_6)_3$	971.15	37.40	2.46	8.67	37.2	2.29	8.66
$[Cr(tpy)_2](PF_6)_3 \cdot 0.1CH_3CN \cdot 1.2H_2O$	977.43	37.08	2.58	8.69	37.06	2.53	8.71
$[Cr(ebzpy)_2](PF_6)_3 \cdot 0.7CH_3CN \cdot 1.2H_2O$	1271.46	44.70	3.62	11.79	44.75	3.68	11.77
$Cr(tpy)Cl_3 \cdot 0.3CH_2Cl_2$	419.22	43.95	3.08	9.87	43.91	2.81	10.02
$Cr(ebzpy)Cl_3 \cdot 0.9CH_2Cl_2$	598.75	47.81	3.97	11.82	47.86	3.83	11.70
$Cr(tppz)Cl_3$	547.63	52.63	3.03	15.39	52.65	2.96	15.35
$Cr(ddpd)Cl_3 \cdot 1.3H_2O$	473.67	43.44	3.94	14.44	43.10	4.18	14.78
$Cr(tpy)(CF_3SO_3)_3 \cdot 1.6H_2O$	732.46	28.39	1.73	5.18	28.38	1.88	5.51
$Cr(tppz)(CF_3SO_3)_3 \cdot 3.3H_2O \cdot 2.5CH_2Cl_2$	887.62	30.37	2.17	7.53	30.51	2.39	7.23
$[Cr(tpy)(ebzpy)](PF_6)_3 \cdot 0.4H_2O$	1094.71	41.70	3.06	10.24	41.69	3.02	10.24
$[Cr(tpy)(tppz)](CF_3SO_3)_3 \cdot 0.3CH_3CN \cdot 1.7H_2O$	1164.21	43.98	2.78	11.17	43.96	2.72	11.19
$[Cr_2Cl_6(tppz)]$	705.13	40.66	2.62	12.31	40.88	2.29	11.92
$[Cr_2Cl_6(bbt)] \cdot H_2O$	799.25	45.00	2.86	10.62	45.08	2.77	10.52
$[Cr_2Cl_6(ebbt)] \cdot 2H_2O$	841.28	45.58	3.14	9.98	45.69	2.88	9.99
$[Cr_2(tpy)_2(bbt)](PF_6)_6 \cdot 2H_2O$	1940.87	40.41	2.45	8.48	40.33	2.36	8.55
$[Cr_2(tpy)_2(bbt)](CF_3SO_3)_6 \cdot 2H_2O$	1965.51	37.19	2.48	8.76	37.13	2.39	8.66
$[Cr_2(tpy)_2(ebbt)](PF_6)_6 \cdot 4H_2O$	2000.93	37.20	2.49	8.35	37.22	2.52	8.40
$[Cr_2(tpy)_2(ebbt)](CF_3SO_3)_6 \cdot 2H_2O$	1989.53	40.88	2.26	8.46	41.05	2.33	8.45

[a] The nature of the solvent molecules are deduced from ^1H NMR and IR spectroscopies and the solvent contents were obtained by multi-linear least-square fits of the experimental %C, % H, %N data.

Table S2 Summary of crystal data, intensity measurements and structure refinements for $[Ga(tpy)_2](PF_6)_3 \cdot 2CH_3CN$ (**1**) and $[Cr(tpy)_2](PF_6)_3 \cdot 2.5CH_3CN$ (**2**)

	$[Ga(tpy)_2](PF_6)_3 \cdot 2CH_3CN$ (**1**)	$[Cr(tpy)_2](PF_6)_3 \cdot 2.5CH_3CN$ (**2**)
Empirical formula	$C_{34}\ H_{28}\ F_{18}\ GaN_8\ P_3$	$C_{35}\ H_{29.50}\ Cr\ F_{18}\ N_{8.50}\ P_3$
Formula weight	1053.27 g/mol	1056.08 g/mol
Temperature	180(2) K	180(2) K
Wavelength	1.54184 Å	1.54184 Å
Crystal System, Space group	Orthorhombic, $P\ 2_1\ 2_1\ 2_1$	Orthorhombic, $P\ b\ c\ a$
Unit cell dimensions	a = 12.8591(2) Å b = 14.0203(2) Å c = 22.3536(4) Å α = 90° β = 90° γ = 90°	a = 22.1556(4) Å b = 32.7297(4) Å c = 47.3405(9) Å α = 90° β = 90° γ = 90°
Volume in Å^3	4030.09(12)	34328.9(10)
Z, Calculated density	4, 1.736 Mg/m^3	32, 1.635 Mg/m^3
Absorption coefficient	3.201 mm^{-1}	4.338 mm^{-1}
F(000)	2104	16960
Theta range for data collection	3.72 to 72.61°	3.05 to 66.60°
Limiting indices	-15<=h<=14, -16<=k<=11, -26<=l<=27	-26<=h<=18, -38<=k<=38, -56<=l<=50
Reflections collected / unique	15078 / 7773 [R(int) = 0.0216]	77193 / 30253 [R(int) = 0.0404]
Completeness to theta	100.0 %	99.7 %
Data / restraints / parameters	7773 / 0 / 569	30253 / 0 / 2345
Goodness-of-fit on F^2	1.047	1.347
Final R indices [I>2σ(I)]	R_1 = 0.0413, ωR_2 = 0.1090	R_1 = 0.0709, ωR_2 = 0.1972
R indices (all data)	R_1 = 0.0419, ωR_2 = 0.1098	R_1 = 0.0963, ωR_2 = 0.2125
Largest diff. peak and hole	0.655 and -0.723e.Å^{-3}	1.242 and -1.224 e.Å^{-3}
Absolute structure parameter	-0.024(19)	-

Table S3 Summary of crystal data, intensity measurements and structure refinements for $[Cr(ebzpy)_2](PF_6)_3 \cdot 5.5CH_3CN$ (**3**) and $[Cr(ebzpy)_2](CF_3SO_3)_3 \cdot 2CH_3CN$ (**4**)

	$[Cr(ebzpy)_2](PF_6)_3 \cdot 5.5CH_3CN$ (**3**)	$[Cr(ebzpy)_2](CF_3SO_3)_3 \cdot 2CH_3CN$ (**4**)
Empirical formula	$C_{114}\,H_{117}\,Cr_2\,F_{36}\,N_{31}\,P_6$	$C_{53}\,H_{48}\,Cr\,F_9\,N_{12}\,O_9\,S_3$
Formula weight	2895.21 g/mol	1316.21 g/mol
Temperature	180(2) K	180(2) K
Wavelength	1.54184 Å	1.54184 Å
Crystal System, Space group	Monoclinic, *P n*	Monoclinic, *C* 2/*c*
Unit cell dimensions	*a* = 11.8436(2) Å *b* = 24.1564(5) Å *c* = 24.5555(5) Å α = 90° β = 99.9231(19)° γ = 90°	*a* = 25.0110(3) Å *b* = 14.00514(16) Å *c* = 33.0269(4) Å α = 90° β = 98.5471(11)° γ = 90°
Volume in Å^3	6920.2(2)	11440.2(2)
Z, Calculated density	2, 1.389 Mg/m^3	8, 1.528 Mg/m^3
Absorption coefficient	2.876 mm^{-1}	3.517 mm^{-1}
F(000)	2960	5400
Theta range for data collection	3.65 to 66.60°	3.57 to 72.64°
Limiting indices	-14<=*h*<=12, -28<=*k*<=27, -14<=*l*<=29	-20<=*h*<=30, -15<=*k*<=17, -40<=*l*<=40
Reflections collected / unique	26563 / 15196 [*R*(int) = 0.0274]	27251 / 11020 [*R*(int) = 0.0218]
Completeness to theta	99.9 %	99.7 %
Data / restraints / parameters	15196 / 3 / 1742	11020 / 0 / 718
Goodness-of-fit on F^2	1.019	1.044
Final *R* indices [$I>2\sigma(I)$]	R_1 = 0.0631, ωR_2 = 0.1733	R_1 = 0.0490, ωR_2 = 0.1298
R indices (all data)	R_1 = 0.0792, ωR_2 = 0.1914	R_1 = 0.0529, ωR_2 = 0.1333
Largest diff. peak and hole	0.704 and -0.467e.Å^{-3}	0.585 and -0.587 e.Å^{-3}
Absolute structure parameter	0.009(8)	-

Table S4 Selected bond distances (Å), bond angles (°) in $[Ga(tpy)_2](PF_6)_3 \cdot 2CH_3CN$ (**1**).

Bond distances (Å)			
Ga(1)-N(5)	1.995(2)	Ga(1)-N(3)	2.080(3)
Ga(1)-N(2)	1.997(2)	Ga(1)-N(6)	2.100(2)
Ga(1)-N(4)	2.077(2)	Ga(1)-N(1)	2.104(2)
Bond angles (°)			
N(5)-Ga(1)-N(2)	178.90(11)	N(4)-Ga(1)-N(6)	156.63(10)
N(5)-Ga(1)-N(4)	79.03(10)	N(3)-Ga(1)-N(6)	92.75(9)
N(2)-Ga(1)-N(4)	101.92(10)	N(5)-Ga(1)-N(1)	102.57(10)
N(5)-Ga(1)-N(3)	100.89(10)	N(2)-Ga(1)-N(1)	78.03(11)
N(2)-Ga(1)-N(3)	78.52(10)	N(4)-Ga(1)-N(1)	89.12(10)
N(4)-Ga(1)-N(3)	95.16(9)	N(3)-Ga(1)-N(1)	156.54(10)
N(5)-Ga(1)-N(6)	77.89(10)	N(6)-Ga(1)-N(1)	92.32(9)
N(2)-Ga(1)-N(6)	101.19(10)		

Table S5 Interplanar angles (°) in $[Ga(tpy)_2](PF_6)_3 \cdot 2CH_3CN$ (**1**). The interplanar angle between the two GaN_3 chelate planes amounts to 88.53°.

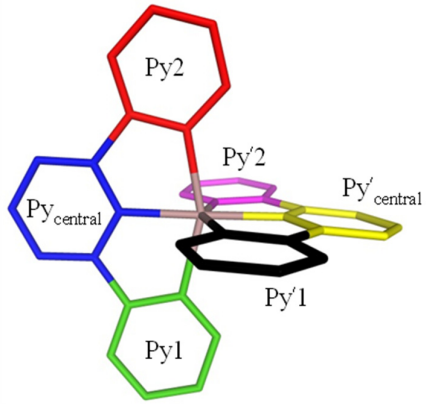

	Py 1	Py 2	Py′central	Py′1	Py′2
Pycentral	3.69°	7.59°	89.13°	81.82°	86.05°
N5C21C22C23C24C25					
Py1		4.20°	88.40°	81.08°	86.61°
N4C16C17C18C19C20					
Py2			84.73°	77.41°	89.82°
N6C26C27C28C29C30					
Py′central				7.32°	5.52°
N2C6C7C8C9C10					
Py′1					12.56°
N1C1C2C3C4C5					

The error is typically ±0.03°.

Table S6 Selected bond distances (Å), bond angles (°) in $[Cr(tpy)_2](PF_6)_3 \cdot 2.5CH_3CN$ (**2**).

Bond distances (Å)			
N(1)-Cr(1)	2.067(4)	N(4)-Cr(1)	2.041(4)
N(2)-Cr(1)	1.987(3)	N(5)-Cr(1)	1.997(4)
N(3)-Cr(1)	2.050(4)	N(6)-Cr(1)	2.083(4)
Bond angles (°)			
N(2)-Cr(1)-N(5)	175.76(18)	N(4)-Cr(1)-N(1)	90.67(17)
N(2)-Cr(1)-N(4)	105.06(17)	N(3)-Cr(1)-N(1)	157.09(15)
N(5)-Cr(1)-N(4)	79.15(19)	N(2)-Cr(1)-N(6)	98.17(16)
N(2)-Cr(1)-N(3)	78.61(15)	N(5)-Cr(1)-N(6)	77.63(18)
N(5)-Cr(1)-N(3)	100.91(15)	N(4)-Cr(1)-N(6)	156.74(17)
N(4)-Cr(1)-N(3)	92.88(16)	N(3)-Cr(1)-N(6)	92.88(15)
N(2)-Cr(1)-N(1)	78.62(15)	N(1)-Cr(1)-N(6)	92.73(16)
N(5)-Cr(1)-N(1)	101.98(16)		

Table S7 Interplanar angles (°) in $[Cr(tpy)_2](PF_6)_3 \cdot 2.5CH_3CN$ (**2**). The average (4 independent molecules) interplanar angle between the two CrN_3 chelate planes amounts to 89.02°.

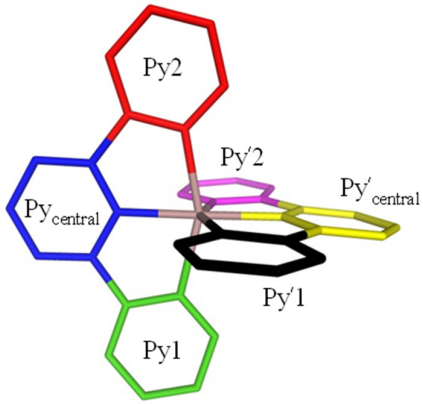

	Py 1	Py 2	Py′central	Py′1	Py′2
Pycentral	2.19°	6.59°	88.60°	84.65°	88.76°
N5C21C22C23C24C25					
Py1		5.60°	89.10°	85.28°	87.96°
N4C16C17C18C19C20					
Py2			85.31°	89.11°	82.37°
N6C26C27C28C29C30					
Py′central				5.33°	8.80°
N2C6C7C8C9C10					
Py′1					8.16°
N1C1C2C3C4C5					

The error is typically ±0.03°.

Table S8 Selected bond distances (Å), bond angles (°) in $[Cr(ebzpy)_2](PF_6)_3 \cdot 5.5CH_3CN$ (**3**).

Bond distances (Å)			
Cr(1B)-N(1B)	2.011(5)	Cr(1B)-N(9B)	2.037(5)
Cr(1B)-N(6B)	2.014(5)	Cr(1B)-N(4B)	2.038(5)
Cr(1B)-N(7B)	2.034(4)	Cr(1B)-N(2B)	2.048(5)
Bond angles (°)			
N(1B)-Cr(1B)-N(6B)	176.9(2)	N(7B)-Cr(1B)-N(4B)	91.92(19)
N(1B)-Cr(1B)-N(7B)	103.02(19)	N(9B)-Cr(1B)-N(4B)	92.6(2)
N(6B)-Cr(1B)-N(7B)	78.31(19)	N(1B)-Cr(1B)-N(2B)	78.18(19)
N(1B)-Cr(1B)-N(9B)	100.4(2)	N(6B)-Cr(1B)-N(2B)	104.61(19)
N(6B)-Cr(1B)-N(9B)	78.27(19)	N(7B)-Cr(1B)-N(2B)	93.98(19)
N(7B)-Cr(1B)-N(9B)	156.6(2)	N(9B)-Cr(1B)-N(2B)	90.9(2)
N(1B)-Cr(1B)-N(4B)	78.53(19)	N(4B)-Cr(1B)-N(2B)	156.7(2)
N(6B)-Cr(1B)-N(4B)	98.66(19)		

Table S9 Interplanar angles (°) in $[Cr(ebzpy)_2](PF_6)_3 \cdot 5.5CH_3CN$ (**3**). The average (two independent molecules) interplanar angle between the two CrN_3 chelate planes amounts to 89.08°.

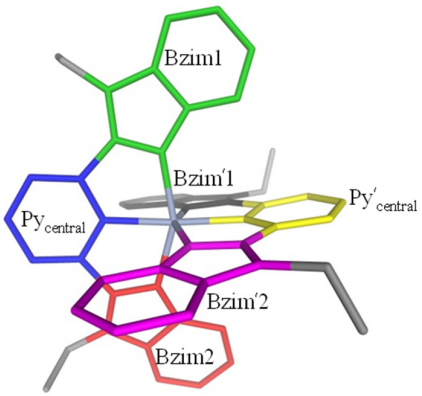

	Bzim1	Bzim2	Py′central	Bzim′1	Bzim′2
Pycentral	1.99 ˚	2.79˚	85.03˚	85.17 ˚	86.19 ˚
N6C31C32C33C34C35					
Bzim1		1.21 ˚	83.20 ˚	83.32 ˚	84.48 ˚
N7C24C25C26C27C28C29N8C30					
Bzim2			83.14 ˚	83.21 ˚	84.58 ˚
N9C36N10C37C38C39C40C41C42					
Py′central				2.07 ˚	7.50 ˚
N1C8C9C10C11C12					
Bzim′1					9.54 ˚
N2C1C2C3C4C5C6N3C7					

The error is typically ±0.03°.

Table S10 Selected bond distances (Å), bond angles (°) in $[Cr(ebzpy)_2](CF_3SO_3)_3 \cdot 2CH_3CN$ (**4**).

Bond distances (Å)			
Cr-N(6)	2.0093(18)	Cr-N(7)	2.0268(19)
Cr-N(1)	2.0185(19)	Cr-N(2)	2.0357(17)
Cr-N(9)	2.0204(19)	Cr-N(4)	2.0383(18)
Bond angles (°)			
N(6)-Cr-N(1)	175.12(7)	N(9)-Cr-N(2)	95.19(7)
N(6)-Cr-N(9)	78.82(7)	N(7)-Cr-N(2)	91.60(7)
N(1)-Cr-N(9)	100.11(7)	N(6)-Cr-N(4)	106.76(7)
N(6)-Cr-N(7)	78.07(7)	N(1)-Cr-N(4)	78.00(8)
N(1)-Cr-N(7)	103.26(8)	N(9)-Cr-N(4)	92.70(8)
N(9)-Cr-N(7)	156.53(8)	N(7)-Cr-N(4)	90.04(8)
N(6)-Cr-N(2)	96.87(7)	N(2)-Cr-N(4)	156.13(8)
N(1)-Cr-N(2)	78.44(7)		

Table S11 Interplanar angles (°) in $[Cr(ebzpy)_2](CF_3SO_3)_3 \cdot 2CH_3CN$ (**4**). The average interplanar angle between the two CrN_3 chelate planes amounts to 90.03°.

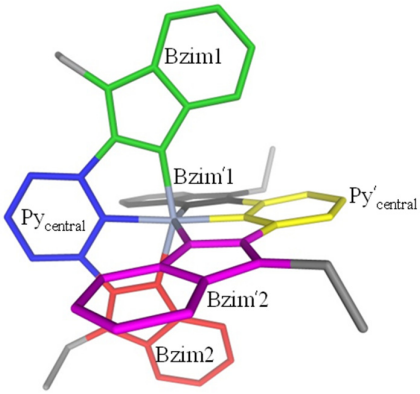

	Bzim1	Bzim2	Py′central	Bzim′1	Bzim′2
Pycentral	9.02˚	3.90˚	89.61˚	82.19˚	77.86˚
N6C31C32C33C34C35					
Bzim1		10.41˚	96.63˚	89.19˚	70.37˚
N7C24C25C26C27C28C29N8C30					
Bzim2			86.68˚	79.25˚	80.54˚
N9C36N10C37C38C39C40C41C42					
Py′central				7.44˚	13.68˚
N1C8C9C10C11C12					
Bzim′1					20.84˚
N2C1C2C3C4C5C6N3C7					

The error is typically ±0.03°.

Table S12 Summary of crystal data, intensity measurements and structure refinements for [Cr(ebzpy)Cl_3]·DMF (**5**) and [Cr(tppz)Cl_3]·2DMF (**6**).

	[Cr(ebzpy)Cl_3]·DMF (**5**)	[Cr(tppz)Cl_3]·2DMF (**6**)
Empirical formula	$C_{26}H_{28}Cl_3CrN_6O$	$C_{30}H_{30}Cl_3CrN_8O_2$
Formula weight	598.89 g/mol	692.97 g/mol
Temperature	180(2) K	180(2) K
Wavelength	1.54184 Å	1.54184 Å
Crystal System, Space group	Monoclinic, $P\,2_1/n$	Monoclinic, $C\,2/c$
Unit cell dimensions	a = 8.32377(13) Å	a = 8.7153(2) Å
	b = 17.0177(3) Å	b = 21.0542(6) Å
	c = 19.4862(3) Å	c = 17.6197(4) Å
	α = 90°	α = 90°
	β = 96.8929(16)°	β = 92.109(2)°
	γ = 90°	γ = 90°
Volume in Å^3	2740.30(8)	3230.92(15)
Z, Calculated density	4, 1.452 Mg/m^3	4, 1.425 Mg/m^3
Absorption coefficient	6.381 mm^{-1}	5.538 mm^{-1}
F(000)	1236	1428
Theta range for data collection	3.46 to 72.56°	4.20 to 72.67°
Limiting indices	-10<=h<=8,	-10<=h<=6,
	-13<=k<=20,	-23<=k<=25,
	-23<=l <=24	-21<=l<=20
Reflections collected / unique	12951 / 5297	7560 / 3119
	[R(int) = 0.0241]	[R(int) = 0.0172]
Completeness to theta	99.9 %	99.8 %
Data / restraints / parameters	5297 / 0 / 338	3119 / 0 / 203
Goodness-of-fit on F^2	1.036	1.064
Final R indices [I>2σ(I)]	R_1 = 0.0333,	R_1 = 0.0326,
	ωR_2 = 0.0904	ωR_2 = 0.0865
R indices (all data)	R_1 = 0.0383,	R_1 = 0.0350,
	ωR_2 = 0.0954	ωR_2 = 0.0886
Largest diff. peak and hole	0.535 and -0.305 e.Å^{-3}	0.595 and -0.654 e.Å^{-3}

Table S13 Selected bond distances (Å), bond angles (°) in [Cr(ebzpy)Cl_3]·DMF (**5**).

Bond distances (Å)			
Cr(1)-N(1)	2.0322(15)	Cr(1)-Cl(2)	2.2958(5)
Cr(1)-N(2)	2.0406(15)	Cr(1)-Cl(3)	2.3293(5)
Cr(1)-N(4)	2.0676(15)	Cr(1)-Cl(1)	2.3443(5)

Symmetry operation (') -*x*+1,*y*,-*z*+1/2.

Bond angles (°)			
N(1)-Cr(1)-N(2)	78.04(6)	N(4)-Cr(1)-Cl(3)	90.40(4)
N(1)-Cr(1)-N(4)	78.01(6)	Cl(2)-Cr(1)-Cl(3)	92.28(2)
N(2)-Cr(1)-N(4)	156.03(6)	N(1)-Cr(1)-Cl(1)	87.90(4)
N(1)-Cr(1)-Cl(2)	178.69(5)	N(2)-Cr(1)-Cl(1)	89.17(5)
N(2)-Cr(1)-Cl(2)	101.45(5)	N(4)-Cr(1)-Cl(1)	88.84(4)
N(4)-Cr(1)-Cl(2)	102.51(4)	Cl(2)-Cr(1)-Cl(1)	93.304(19)
N(1)-Cr(1)-Cl(3)	86.51(5)	Cl(3)-Cr(1)-Cl(1)	174.40(2)
N(2)-Cr(1)-Cl(3)	89.27(5)		

Table S14 Interplanar angles (°) in [Cr(ebzpy)Cl_3]·DMF (**5**). The interplanar angle between the chelate CrN_3 plane and the CrCl3 plane amounts to 89.62°.

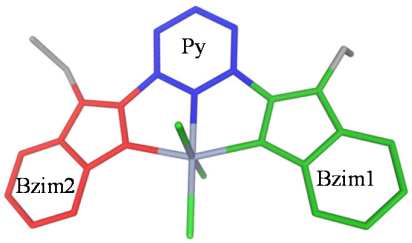

	Bzim1	Bzim2	Cr-$Cl_{central}$ -Cl1	Cr-$Cl_{central}$ -Cl2
Py N1C8C9C10C11C12	1.92˚	10.60˚	89.89˚	89.65˚
Bzim1 C1C2C3C4C5C6N3C7N2		9.12˚	89.59˚	89.13˚
Bzim2 C13N5C14C15C16C17C18C19N4			81.78˚	81.32˚
$Cl_{central}$ - Cl 1				0.45˚

The error is typically ±0.03°.

Table S15 Selected bond distances (Å), bond angles (°) in [Cr(tppz)Cl_3]·2DMF (**6**).

Bond distances (Å)			
Cr(1)-N(2)	2.005(2)	Cr(1)-Cl(2)	2.2924(7)
Cr(1)-N(1)#1	2.0677(15)	Cr(1)-Cl(1)	2.3214(4)
Cr(1)-N(1)	2.0677(15)	Cr(1)-Cl(1)#1	2.3215(4)

Symmetry operation (') -*x*+1,*y*,-*z*+1/2.

Bond angles (°)			
N(2)-Cr(1)-N(1)#1	78.26(4)	N(1)-Cr(1)-Cl(1)	89.34(4)
N(2)-Cr(1)-N(1)	78.26(4)	Cl(2)-Cr(1)-Cl(1)	92.007(14)
N(1)#1-Cr(1)-N(1)	156.51(9)	N(2)-Cr(1)-Cl(1)#1	87.992(14)
N(2)-Cr(1)-Cl(2)	180.0	N(1)#1-Cr(1)-Cl(1)#1	89.34(4)
N(1)#1-Cr(1)-Cl(2)	101.74(4)	N(1)-Cr(1)-Cl(1)#1	89.84(4)
N(1)-Cr(1)-Cl(2)	101.74(4)	Cl(2)-Cr(1)-Cl(1)#1	92.008(14)
N(2)-Cr(1)-Cl(1)	87.993(14)	Cl(1)-Cr(1)-Cl(1)#1	175.99(3)
N(1)#1-Cr(1)-Cl(1)	89.84(4)		

Table S16 Interplanar angles (°) in [Cr(tppz)Cl_3]·2DMF (**6**). The interplanar angle between the chelate CrN_3 plane and the $CrCl_3$ plane amounts to 89.75˚.

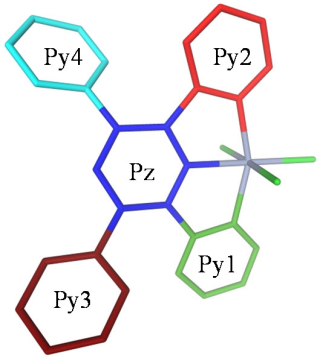

	Py1	Py2	Py3	Py4
$Pz^{central}$ N2C6C7N3C#7C#6	19.46˚	19.46˚	33.42˚	33.42˚
Py1 N#1C#1C#2C#3C#4C#5		0.54˚	51.42˚	51.58˚
Py2 N1C1C2C3C4C5			51.58˚	51.42˚
Py3 N4C8C9C10C11C12				28.25˚

The error is typically ±0.03°.

Table S17 Summary of crystal data, intensity measurements and structure refinements for $[H_2(ebzpy)](CF_3SO_3)_2$ (**10**) and $[Cr(tpy)(ebzpy)](PF_6)_3 \cdot 2CH_3CN$ (**7**).

	$[H_2(ebzpy)](CF_3SO_3)_2$ (**10**)	$[Cr(tpy)(ebzpy)](PF_6)_3 \cdot 2CH_3CN$ (**7**)
Empirical formula	$C_{25}H_{23}F_6N_5O_6S_2$	$C_{42}H_{38}CrF_{18}N_{10}P_3$
Formula weight	667.60 g/mol	1169.73 g/mol
Temperature	180(2) K	180(2) K
Wavelength	1.54184 Å	1.54184 Å
Crystal System, Space group	Monoclinic, *I* 2/a	Monoclinic, *P* $2_1/n$
Unit cell dimensions	*a* = 15.8830(3) Å	*a* = 8.50371(9) Å
	b = 20.6312(4) Å	*b* = 21.3589(3) Å
	c = 17.6293(4) Å	*c* = 26.1354(3) Å
	$\alpha = 90°$	$\alpha = 90°$
	$\beta = 105.672(2)°$	$\beta = 93.6609(10)°$
	$\gamma = 90°$	$\gamma = 90°$
Volume in Å^3	5562.1(2)	4737.29(9)
Z, Calculated density	8, 1.594 Mg/m^3	4, 1.640 Mg/m^3
Absorption coefficient	2.572 mm^{-1}	4.005 mm^{-1}
F(000)	2736	2364
Theta range for data collection	3.372 to 72.557°	3.39 to 72.58°
Limiting indices	-19<=*h*<=18, -22<=*k*<=25, -21<=*l*<=16	-10<=*h*<=10, -17<=*k*<=26, -32<=*l*<=19
Reflections collected / unique	15572 / 5372 [*R*(int) = 0.0172]	21914 / 9149 [*R*(int) = 0.0236]
Completeness to theta	99.8 %	99.9 %
Data / restraints / parameters	5372 / 2 / 465	9149 / 0 / 671
Goodness-of-fit on F^2	1.058	1.044
Final *R* indices [$I>2\sigma(I)$]	R_1 = 0.0710, ωR_2 = 0.1928	R_1 = 0.0537, ωR_2 = 0.1460
R indices (all data)	R_1 = 0.0794, ωR_2 = 0.2015	R_1 = 0.0582, ωR_2 = 0.1506
Largest diff. peak and hole	1.465 and -1.370 e.Å^{-3}	1.795 and -0.637e.Å^{-3}

Table S18 Selected bond distances (Å), bond angles (°) and hydrogen bonds in $[H_2(ebzpy)](CF_3SO_3)_2$ (**10**). The dihedral angles between the adjacent benzimidazole and pyridine rings amount to 12.89° and 13.24°. The dihedral angle between the two benzimidazole rings is 2.45°.

Bond distances (Å)			
N(1)-H(1)	0.8800	N(4)-H(4)	0.8800
C(7)-C(8)	1.474(4)	C(12)-C(13)	1.476(4)

Bond angles (°)			
N(3)-C(8)-C(7)	113.2(3)	N(3)-C(12)-C(13)	113.2(3)
C(9)-C(8)-C(7)	123.8(3)	C(11)-C(12)-C(13)	124.0(3)

Hydrogen bonds				
D-H...A	d(D-H)	d(H...A)	d(D...A)	<(DHA)
N(1)-H(1)...O(3) [a]	0.88 Å	1.95 Å	2.813(4) Å	166.8°
N(4)-H(4)...O(3) [a]	0.88 Å	1.98 Å	2.835(3) Å	164.4°

[a] The oxygen atom belongs to the triflate anion which is hydrogen bound to the two protonated nitrogen atoms of the ligand.

Table S19 Selected bond distances (Å), bond angles (°) in [Cr(tpy)(ebzpy)]$(PF_6)_3 \cdot 2CH_3CN$ (**7**).

Bond distances (Å)			
Cr(1)-N(7)	1.990(2)	Cr(1)-N(1)	2.047(2)
Cr(1)-N(3)	2.025(2)	Cr(1)-N(6)	2.067(2)
Cr(1)-N(4)	2.036(2)	Cr(1)-N(8)	2.074(2)
Bond angles (°)			
N(7)-Cr(1)-N(3)	178.03(9)	N(4)-Cr(1)-N(6)	95.86(9)
N(7)-Cr(1)-N(4)	100.07(8)	N(1)-Cr(1)-N(6)	89.18(9)
N(3)-Cr(1)-N(4)	78.21(8)	N(7)-Cr(1)-N(8)	78.24(9)
N(7)-Cr(1)-N(1)	103.90(8)	N(3)-Cr(1)-N(8)	102.64(9)
N(3)-Cr(1)-N(1)	77.82(8)	N(4)-Cr(1)-N(8)	89.19(8)
N(4)-Cr(1)-N(1)	156.03(8)	N(1)-Cr(1)-N(8)	95.43(8)
N(7)-Cr(1)-N(6)	78.40(9)	N(6)-Cr(1)-N(8)	156.61(9)
N(3)-Cr(1)-N(6)	100.75(9)		

Table S20 Interplanar angles (°) in [Cr(tpy)(ebzpy)]$(PF_6)_3 \cdot 2CH_3CN$ (**7**). The interplanar angle between the two chelate CrN_3 planes amounts to 86.68˚.

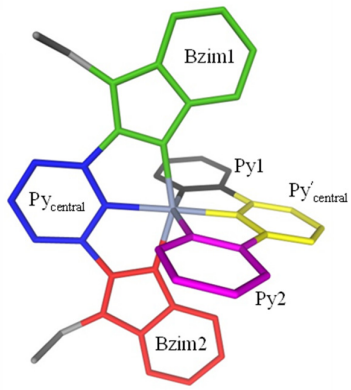

	Bzim1 (ebzpy)	Bzim2 (ebzpy)	Py′central (tpy)	Py1 (tpy)	Py2 (tpy)
Pycentral N3C8C9C10C11C12	5.75˚	5.37˚	85.24˚	78.61˚	84.05˚
Bzim1 N4C13N5C14C15C16C17C18C19		2.45˚	79.96˚	73.06˚	78.72˚
Bzim2 N1C1C2C3C4C5C6N2C7			81.68˚	74.52˚	80.41˚
Py′central N7C29C30C31C32C33				10.55˚	1.66˚
Py1 N6C24C25C26C27C28					8.91˚

The error is typically ±0.03°.

Table S21 Summary of crystal data, intensity measurements and structure refinements for $[Cr(tpy)(tppz)](PF_6)_3 \cdot 3CH_3CN$ (**8**) and $[Cr(tpy)(tppz)](CF_3SO_3)_3 \cdot CH_3CN$ (**9**)

	$[Cr(tpy)(tppz)](PF_6)_3 \cdot 3CH_3CN$ (**8**)	$[Cr(tpy)(tppz)](CF_3SO_3)_3 \cdot CH_3CN$ (**9**)
Empirical formula	$C_{45}\ H_{36}\ Cr\ F_{18}\ N_{12}\ P_3$	$C_{44}\ H_{30}\ Cr\ F_9\ N_{10}\ O_9\ S_3$
Formula weight	1231.77 g/mol	1161.96 g/mol
Temperature	180(2) K	180(2) K
Wavelength	1.54184 Å	1.54184 Å
Crystal System, Space group	Monoclinic, *P* 21/*c*	Triclinic ,*P* -1
Unit cell dimensions	*a* = 12.7176(5) Å	*a* = 9.6733(4) Å
	b = 43.7623(13) Å	*b* = 15.2234(6) Å
	c = 9.3910(3) Å	*c* = 16.4990(5) Å
	α = 90°	α = 102.661(3)°
	β = 102.712(4)°	β = 90.539(3)°
	γ = 90°	γ = 94.791(3)°
Volume in Å^3	5098.5(3)	2361.31(16)
Z, Calculated density	4, 1.605 Mg/m^3	2, 1.634 Mg/m^3
Absorption coefficient	3.770 mm^{-1}	4.162 mm^{-1}
F(000)	2484	1178
Theta range for data collection	3.70 to 72.54°	3.58 to 72.61°
Limiting indices	-14<=*h*<=15, -49<=*k*<=53, -11<=*l*<=11	-11<=*h*<=10, -18<=*k*<=18, -15<=*l*<=20
Reflections collected / unique	18695 / 9847 [*R*(int) = 0.0251]	15832 / 9095 [*R*(int) = 0.0275]
Completeness to theta	99.8 %	99.9 %
Data / restraints / parameters	9847 / 0 / 715	9095 / 31 / 687
Goodness-of-fit on F^2	1.025	1.049
Final *R* indices [$I>2\sigma(I)$]	R_1 = 0.0567, ωR_2 = 0.1398	R_1 = 0.0776, ωR_2 = 0.2203
R indices (all data)	R_1 = 0.0727, ωR_2 = 0.1506	R_1 = 0.0845, ωR_2 = 0.2315
Largest diff. peak and hole	0.720 and -0.441 e.Å^{-3}	1.902 and -0.899 e.Å^{-3}

Table S22 Selected bond distances (Å), bond angles (°) in $[Cr(tpy)(tppz)](PF_6)_3 \cdot 3CH_3CN$ (**8**).

Bond distances (Å)			
Cr(1)-N(2)	1.984(3)	Cr(1)-N(6)	2.057(3)
Cr(1)-N(5)	1.998(2)	Cr(1)-N(1)	2.062(3)
Cr(1)-N(4)	2.051(3)	Cr(1)-N(3)	2.062(3)
Bond angles (°)			
N(2)-Cr(1)-N(5)	176.91(11)	N(4)-Cr(1)-N(1)	94.53(10)
N(2)-Cr(1)-N(4)	104.72(11)	N(6)-Cr(1)-N(1)	92.01(10)
N(5)-Cr(1)-N(4)	78.35(10)	N(2)-Cr(1)-N(3)	78.44(11)
N(2)-Cr(1)-N(6)	98.10(10)	N(5)-Cr(1)-N(3)	102.10(11)
N(5)-Cr(1)-N(6)	78.85(10)	N(4)-Cr(1)-N(3)	90.10(10)
N(4)-Cr(1)-N(6)	157.08(11)	N(6)-Cr(1)-N(3)	92.39(11)
N(2)-Cr(1)-N(1)	78.65(11)	N(1)-Cr(1)-N(3)	157.06(11)
N(5)-Cr(1)-N(1)	100.84(10)		

Table S23 Interplanar angles (°) in $[Cr(tpy)(tppz)](PF_6)_3 \cdot 3CH_3CN$ (**8**). The interplanar angle between the two chelate CrN_3 planes amounts to 88.66˚.

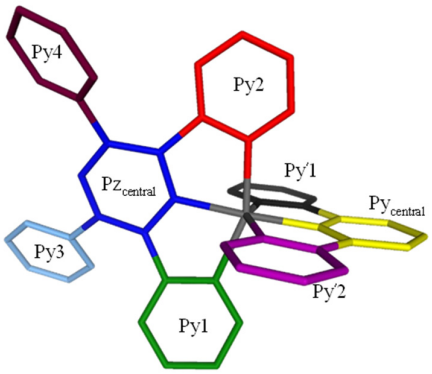

	Py1 tppz)	Py2 (tppz)	Py3 (tppz)	Py4 (tppz)	$Py_{central}$ (tpy)	Py1 (tpy)	Py2 (tpy)
$Pz_{central}$ N5C21C28N7C34C22	16.48˚	22.56˚	38.34˚	24.34˚	79.50˚	80.42˚	77.96˚
Py1 C20N4C16C17C18C19		6.95˚	54.02˚	40.64˚	85.08˚	83.93˚	86.31˚
Py2 N6C23C24C25C26C27			58.68˚	46.90˚	78.32˚	77.25˚	79.66˚
Py3 C29C30C31C32C33N8				21.07˚	53.14˚	52.74˚	50.24˚
Py4 C35C36C37C38C39N9					55.61˚	56.34˚	53.84˚
$Py_{central}$ N2C6C7C8C9C10						9.13˚	3.48˚
Py′1 N3C11C12C13C14C15							11.26˚

The error is typically ±0.03°.

Table S24 Selected bond distances (Å), bond angles (°) in $[Cr(tpy)(tppz)](CF_3SO_3)_3 \cdot CH_3CN$ (**9**).

Bond distances (Å)			
Cr(1)-N(2)	1.992(3)	Cr(1)-N(3)	2.049(3)
Cr(1)-N(5)	1.997(3)	Cr(1)-N(1)	2.061(3)
Cr(1)-N(6)	2.046(3)	Cr(1)-N(4)	2.067(3)
Bond angles (°)			
N(2)-Cr(1)-N(5)	178.01(12)	N(6)-Cr(1)-N(1)	95.32(12)
N(2)-Cr(1)-N(6)	102.80(13)	N(3)-Cr(1)-N(1)	156.84(14)
N(5)-Cr(1)-N(6)	78.78(12)	N(2)-Cr(1)-N(4)	99.92(13)
N(2)-Cr(1)-N(3)	78.31(13)	N(5)-Cr(1)-N(4)	78.55(12)
N(5)-Cr(1)-N(3)	102.97(13)	N(6)-Cr(1)-N(4)	157.16(13)
N(6)-Cr(1)-N(3)	89.56(12)	N(3)-Cr(1)-N(4)	92.83(12)
N(2)-Cr(1)-N(1)	78.53(12)	N(1)-Cr(1)-N(4)	91.36(12)
N(5)-Cr(1)-N(1)	100.19(12)		

Table S25 Interplanar angles (°) in [Cr(tpy)(tppz)](CF$_3$SO$_3$)$_3$·CH$_3$CN (**9**). The interplanar angle between the two chelate CrN$_3$ planes amounts to 88.08˚.

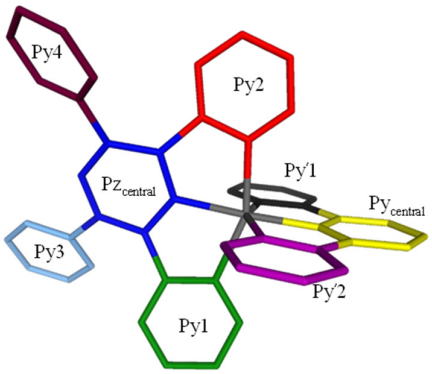

	Py1 (tppz)	Py2 (tppz)	Py3 (tppz)	Py4 (tppz)	Py$_{central}$ (tpy)	Py1 (tpy)	Py2 (tpy)
Pz$_{central}$ N5C21C28N7C34C22	19.25˚	15.28˚	31.38˚	31.27˚	79.98˚	85.38˚	85.61˚
Py1 C20N4C16C17C18C19		6.30˚	49.19˚	50.32˚	80.88˚	75.65˚	75.17˚
Py2 N6C23C24C25C26C27			46.47˚	45.37˚	84.98˚	79.45˚	79.53˚
Py3 C29C30C31C32C33N8				19.40˚	51.18˚	55.17˚	57.40˚
Py4 C35C36C37C38C39N9					50.34˚	56.33˚	55.35˚
Py$_{central}$ N2C6C7C8C9C10						6.40˚	6.43˚
Py′1 N3C11C12C13C14C15							6.59˚

The error is typically ±0.03°.

Table S26 Summary of crystal data, intensity measurements and structure refinements for $[Cr_2Cl_6(tppz)]\cdot 3C_5H_9NO$ (**11**) and $[Cr_2Cl_6(bbt)]$ (**12**).

	$[Cr_2Cl_6(tppz)]\cdot 3C_5H_9NO$ (**11**)	$[Cr_2Cl_6(bbt)]$ (**12**)
Empirical formula	$C_{39}H_{43}Cl_6Cr_2N_9O_3$	$C_{30}H_{20}Cl_6Cr_2N_6$
Formula weight	1002.52 g/mol	781.22 g/mol
Temperature	180.1(3) K	179.9(3)
Radiation (Wavelength)	CuKα (λ = 1.5418 Å)	CuKα (λ = 1.5418 Å)
Crystal System, Space group	Trigonal, $P3_2$	Tetragonal, $P4_12_12$
Unit cell dimensions	a = 18.90091(13) Å b = 18.90091(13) Å c = 21.1210(2) Å α = 90° β = 90° γ = 120°	a = 13.61144(9) Å b = 13.61144(9) Å c = 24.0699(3) Å α = 90° β = 90° γ = 90°
Volume in Å^3	6534.46(12)	4459.46(7)
Z, Calculated density	6, 1.529 g/cm^3	4, 1.164 g/cm^3
Absorption coefficient	7.901 mm^{-1}	7.516 mm^{-1}
F(000)	3084.0	1568.0
Crystal size (mm^3)	0.2869 × 0.0997 × 0.027	0.2849 × 0.2198 × 0.1444
Theta range for data collection	6.832° to 146.842°	7.462° to 146.704°
Limiting indices	$-20 \le h \le 23$, $-23 \le k \le 22$, $-25 \le l \le 23$	$-15 \le h \le 16$, $-16 \le k \le 13$, $-29 \le l \le 29$
Reflections collected	63252	40446
Independent reflections	16355 [R_{int} = 0.0790, R_{sigma} = 0.0649]	4468 [R_{int} = 0.0711, R_{sigma} = 0.0271]
Data / restraints / parameters	16355/1/1072	4468/0/200
Goodness-of-fit on F^2	1.026	1.060
Final R indices [I>2σ(I)]	R_1 = 0.0462, wR_2 = 0.1114	R_1 = 0.0338, wR_2 = 0.0902
R indices (all data)	R_1 = 0.0501, wR_2 = 0.1140	R_1 = 0.0358, wR_2 = 0.0917
Largest diff. peak and hole	0.50/-0.51 e.Å^{-3}	0.22/-0.31 e.Å^{-3}

Table S27 Selected bond distances (Å), bond angles (°) in $[Cr_2Cl_6(tppz)]\cdot 3C_5H_9NO$ (**11**).

Bond distances (Å)			
Cr(1)-N(4)	2.054(7)	Cr(1)-Cl(1)	2.325(3)
Cr(1)-N(5)	2.018(6)	Cr(1)-Cl(2)	2.277(2)
Cr(1)-N(6)	2.065(7)	Cr(1)-Cl(3)	2.320(3)
Cr(2)-N(1)	2.067(7)	Cr(2)-Cl(4)	2.318(3)
Cr(2)-N(2)	2.015(7)	Cr(2)-Cl(5)	2.278(2)
Cr(2)-N(3)	2.062(7)	Cr(2)-Cl(6)	2.323(3)
Cr(3)-N(31)	2.063(7)	Cr(3)-Cl(10)	2.328(3)
Cr(3)-N(32)	2.014(7)	Cr(3)-Cl(11)	2.279(2)
Cr(3)-N(33)	2.062(7)	Cr(3)-Cl(12)	2.299(3)
Cr(4)-N(34)	2.070(6)	Cr(4)-Cl(7)	2.321(3)
Cr(4)-N(35)	2.014(6)	Cr(4)-Cl(8)	2.272(2)
Cr(4)-N(36)	2.065(7)	Cr(4)-Cl(9)	2.327(3)
Bond angles (°)			
Cl(3)-Cr(1)-Cl(1)	174.89(9)	Cl(5)-Cr(2)-Cl(6)	91.20(9)
Cl(2)-Cr(1)-Cl(1)	91.53(10)	Cl(5)-Cr(2)-Cl(4)	93.38(9)
Cl(2)-Cr(1)-Cl(3)	93.57(9)	Cl(4)-Cr(2)-Cl(6)	175.40(9)
N(4)-Cr(1)-Cl(1)	91.1(2)	N(2)-Cr(2)-Cl(5)	176.8(2)
N(4)-Cr(1)-Cl(3)	87.9(2)	N(2)-Cr(2)-Cl(6)	85.8(2)
N(4)-Cr(1)-Cl(2)	101.70(19)	N(2)-Cr(2)-Cl(4)	89.6(2)
N(4)-Cr(1)-N(6)	157.3(3)	N(2)-Cr(2)-N(1)	78.2(2)
N(5)-Cr(1)-Cl(1)	86.0(2)	N(2)-Cr(2)-N(3)	78.7(2)
N(5)-Cr(1)-Cl(3)	88.9(2)	N(1)-Cr(2)-Cl(5)	100.78(18)
N(5)-Cr(1)-Cl(2)	177.5(2)	N(1)-Cr(2)-Cl(6)	90.6(2)
N(5)-Cr(1)-N(4)	78.0(2)	N(1)-Cr(2)-Cl(4)	89.0(2)
N(5)-Cr(1)-N(6)	79.5(2)	N(3)-Cr(2)-Cl(5)	102.41(18)
N(6)-Cr(1)-Cl(1)	89.6(2)	N(3)-Cr(2)-Cl(6)	89.7(2)
N(6)-Cr(1)-Cl(3)	89.4(2)	N(3)-Cr(2)-Cl(4)	88.9(2)
N(6)-Cr(1)-Cl(2)	100.94(19)	N(3)-Cr(2)-N(1)	156.8(2)
Cl(12)-Cr(3)-Cl(10)	175.27(9)	Cl(7)-Cr(4)-Cl(9)	174.31(9)
Cl(11)-Cr(3)-Cl(12)	92.79(10)	Cl(8)-Cr(4)-Cl(7)	91.12(9)

Cl(11)-Cr(3)-Cl(10)	91.69(10)	Cl(8)-Cr(4)-Cl(9)	94.44(9)
N(33)-Cr(3)-Cl(12)	88.9(2)	N(36)-Cr(4)-Cl(7)	92.3(2)
N(33)-Cr(3)-Cl(10)	91.7(2)	N(36)-Cr(4)-Cl(8)	99.95(18)
N(33)-Cr(3)-Cl(11)	100.5(2)	N(36)-Cr(4)-Cl(9)	88.0(2)
N(33)-Cr(3)-N(31)	156.9(3)	N(36)-Cr(4)-N(34)	157.5(2)
N(31)-Cr(3)-Cl(12)	89.0(2)	N(35)-Cr(4)-Cl(7)	85.4(2)
N(31)-Cr(3)-Cl(10)	88.5(2)	N(35)-Cr(4)-Cl(8)	176.3(2)
N(31)-Cr(3)-Cl(11)	102.6(2)	N(35)-Cr(4)-Cl(9)	89.1(2)
N(32)-Cr(3)-Cl(12)	89.1(2)	N(35)-Cr(4)-N(36)	79.1(3)
N(32)-Cr(3)-Cl(10)	86.5(2)	N(35)-Cr(4)-N(34)	78.5(2)
N(32)-Cr(3)-Cl(11)	177.9(2)	N(34)-Cr(4)-Cl(7)	88.2(2)
N(32)-Cr(3)-N(33)	78.6(3)	N(34)-Cr(4)-Cl(8)	102.58(17)
N(32)-Cr(3)-N(31)	78.3(2)	N(34)-Cr(4)-Cl(9)	89.4(2)

Table S28 Interplanar angles (°) in $[Cr_2Cl_6(tppz)]\cdot 3C_5H_9NO$ (**11**). The interplanar angle between the two chelate CrN_3 planes amounts to 25.2(2)° in a and 25.6(2)° in b.

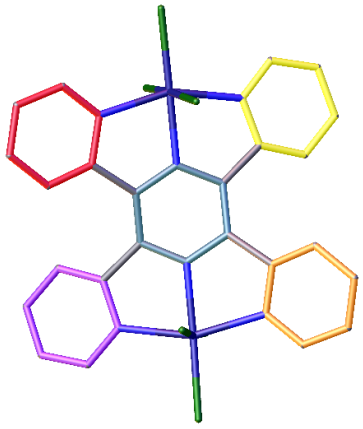

There are two independent complexes in the asymmetric unit that can be overlaid.

Complex a

Py1 N33 C44 C45 C46 C47 C48

Py2 N36 C56 C57 C58 C59 C60

Pz1 N32 C43 C42 C54 C55 N35

Py3 N31 C37 C38 C39 C40 C41

Py4 N34 C49 C50 C51 C52 C53

	Py1	Py2	Pz1	Py4	Py4
Py1		42.4	17.6	8.3	39.3
Py2			24.9	46.8	5.1
Pz1				22.3	22.1
Py3					44.4

Complex b

Py1 N4 C19 C20 C21 C22 C23

Py2 N1 C7 C8 C9 C10 C11

Pz1 N2 C12 C24 N5 C25 C13

Py3 N6 C26 C27 C28 C29 C30

Py4 N3 C14 C15 C16 C17 C18

	Py1	Py2	Pz1	Py4	Py4
Py1		39.1	16.8	9.2	37.7
Py2			22.5	47.7	1.44
Pz1				25.2	21.0
Py3					46.2

The error is typically ±0.3°.

Table S29 Selected bond distances (Å), bond angles (°) in $[Cr_2Cl_6(bbt)]$ (**12**).

Bond distances (Å)			
Cr(1)-N(1)	2.089(4)	Cr(1)-Cl(1)	2.2853(10)
Cr(1)-N(2)	1.999(3)	Cr(1)-Cl(2)	2.3384(10)
Cr(1)-N(3)	2.073(3)	Cr(1)-Cl(3)	2.3090(11)
Bond angles (°)			
Cl(3)-Cr(1)-Cl(2)	174.75(4)	N(3)-Cr(1)-Cl(3)	87.99(9)
Cl(1)-Cr(1)-Cl(3)	92.74(4)	N(3)-Cr(1)-Cl(2)	89.51(9)
Cl(1)-Cr(1)-Cl(2)	92.31(4)	N(3)-Cr(1)-Cl(1)	102.79(9)
N(2)-Cr(1)-Cl(3)	88.26(9)	N(3)-Cr(1)-N(1)	156.27(11)
N(2)-Cr(1)-Cl(2)	86.71(9)	N(1)-Cr(1)-Cl(3)	90.40(9)
N(2)-Cr(1)-Cl(1)	178.50(9)	N(1)-Cr(1)-Cl(2)	90.02(9)
N(2)-Cr(1)-N(3)	78.36(12)	N(1)-Cr(1)-Cl(1)	100.94(9)
N(2)-Cr(1)-N(1)	77.93(12)		

Table S30 Interplanar angles (°) in $[Cr_2Cl_6(bbt)]$ (**12**). The interplanar angle between the two chelate CrN_3 planes of the unit amounts to 40.9(1)°.

The two halves of the complexes are related by symmetry.

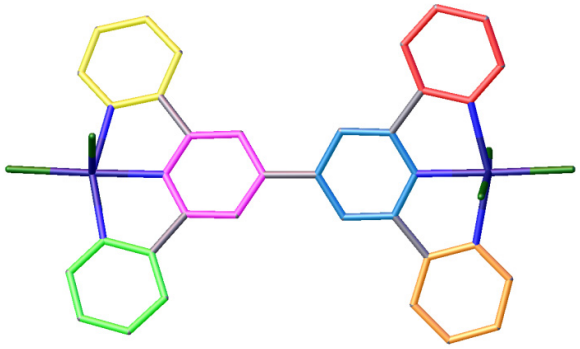

Symmetry equivalent planes generated by the symmetry operator (1-y, 1-x, 3/2-z)

Py1	Py1’	N1 C4 C5 C6 C7 C8
Py2	Py2’	N2 C9 C10 C11 C12 C13
Py3	Py3’	N3 C14 C15 C16 C17 C18

	Py2	Py3	Py1’	Py2’	Py3’
Py1	3.4	7.8	43.0	39.6	39.0
Py2		6.2	39.6	36.2	35.6
Py3			39.0	35.6	33.9
Py1’				3.4	7.8
Py2’					6.2

*table is redundant due to the symmetry relationship between the Py and Py’ planes

Typical errors are ±0.2°.

Table S31 Summary of crystal data, intensity measurements and structure refinements for $[Cr_2(tpy)_2(bbt)](PF_6)_6{\cdot}8CH_3CN{\cdot}(CH_3CH_2)_2O$ (**13**) and $[Cr_2(tpy)_2(ebbt)](PF_6)_6{\cdot}10CH_3CN$ (**14**).

	$[Cr_2(tpy)_2(bbt)](PF_6)_6$ $\cdot 8CH_3CN\cdot(CH_3CH_2)_2O$ (**13**)	$[Cr_2(tpy)_2(ebbt)](PF_6)_6$ $\cdot 10CH_3CN$ (**14**)
Empirical formula	$C_{80}H_{76}Cr_2F_{36}N_{20}OP_6$	$C_{82}H_{72}Cr_2F_{36}N_{22}P_6$
Formula weight	2307.42 g/mol	2339.43 g/mol
Temperature	212(40) K	180.00(14) K
Radiation (Wavelength)	CuKα (λ = 1.5418 Å)	CuKα (λ = 1.54184 Å)
Crystal System, Space group	triclinic, *P*-1	triclinic, *P*-1
Unit cell dimensions	*a* = 11.6319(3) Å	*a* = 10.18638(16) Å
	b = 20.7157(5) Å	*b* = 12.5709(2) Å
	c = 22.6001(5) Å	*c* = 21.0644(3) Å
	α = 65.495(2)°	α = 104.2876(14)°
	β = 82.9117(19)°	β = 90.8897(12)°
	γ = 81.9267(19)°	γ = 104.2657(14)°
Volume in Å^3	4893.3(2)	2524.92(7)
Z, Calculated density	2, 1.566 g/cm^3	1, 1.539 g/cm^3
Absorption coefficient	3.875 mm^{-1}	3.764 mm^{-1}
F(000)	2332.0	1180.0
Crystal size (mm^3)	0.8178 × 0.2444 × 0.0329	0.679 × 0.222 × 0.126
Theta range for data collection	7.564° to 146.852°	7.512° to 147.434°
Limiting indices	$-14 \le h \le 14$,	$-11 \le h \le 12$,
	$-25 \le k \le 25$,	$-15 \le k \le 15$,
	$-28 \le l \le 28$	$-26 \le l \le 26$
Reflections collected	69658	39775
Independent reflections	18913 [R_{int} = 0.0542, R_{sigma} = 0.0427]	10061 [R_{int} = 0.0306, R_{sigma} = 0.0208]
Data / restraints / parameters	18913/468/1371	10061/328/790
Goodness-of-fit on F^2	1.051	1.074
Final *R* indices [$I>2\sigma(I)$]	R_1 = 0.0575, wR_2 = 0.1547	R_1 = 0.0518, wR_2 = 0.1460
R indices (all data)	R_1 = 0.0666, wR_2 = 0.1636	R_1 = 0.0590, wR_2 = 0.1535
Largest diff. peak and hole	0.93/-0.65 e.Å^{-3}	0.59/-0.43 e.Å^{-3}

Table S32 Selected bond distances (Å), bond angles (°) in $[Cr_2(tpy)_2(bbt)](PF_6)_6 \cdot 8CH_3CN \cdot (CH_3CH_2)_2O$ (**13**).

Bond distances (Å)			
Cr(1)-N(1)	2.062(2)	Cr(1)-N(21)	2.057(2)
Cr(1)-N(2)	1.998(2)	Cr(1)-N(22)	1.994(2)
Cr(1)-N(3)	2.062(2)	Cr(1)-N(23)	2.067(2)
Cr(3)-N(41)	2.059(2)	Cr(3)-N(61)	2.064(2)
Cr(3)-N(42)	1.986(2)	Cr(3)-N(62)	1.985(2)
Cr(3)-N(43)	2.063(2)	Cr(3)-N(63)	2.057(2)
Bond angles (°)			
N(3)-Cr(1)-N(23)	92.94(9)	N(42)-Cr(3)-N(43)	78.74(9)
N(2)-Cr(1)-N(3)	78.60(9)	N(42)-Cr(3)-N(61)	98.10(9)
N(2)-Cr(1)-N(1)	78.13(9)	N(42)-Cr(3)-N(41)	78.34(9)
N(2)-Cr(1)-N(23)	100.15(8)	N(42)-Cr(3)-N(63)	104.44(8)
N(2)-Cr(1)-N(21)	103.47(8)	N(43)-Cr(3)-N(61)	93.27(9)
N(1)-Cr(1)-N(3)	156.71(9)	N(62)-Cr(3)-N(42)	176.55(9)
N(1)-Cr(1)-N(23)	90.45(9)	N(62)-Cr(3)-N(43)	102.89(9)
N(22)-Cr(1)-N(3)	98.17(9)	N(62)-Cr(3)-N(61)	78.81(9)
N(22)-Cr(1)-N(2)	176.27(9)	N(62)-Cr(3)-N(41)	100.07(9)
N(22)-Cr(1)-N(1)	105.07(9)	N(62)-Cr(3)-N(63)	78.60(9)
N(22)-Cr(1)-N(23)	78.06(8)	N(41)-Cr(3)-N(43)	157.04(8)
N(22)-Cr(1)-N(21)	78.42(8)	N(41)-Cr(3)-N(61)	91.30(9)
N(21)-Cr(1)-N(3)	92.72(9)	N(63)-Cr(3)-N(43)	92.77(9)
N(21)-Cr(1)-N(1)	93.34(9)	N(63)-Cr(3)-N(61)	157.39(9)
N(21)-Cr(1)-N(23)	156.36(8)	N(63)-Cr(3)-N(41)	91.57(9)

Table S33 Interplanar angles (°) in $[Cr_2(tpy)_2(bbt)](PF_6)_6 \cdot 8CH_3CN \cdot (CH_3CH_2)_2O$ (**13**). The interplanar angle between the two chelate CrN_3 planes of bridging the back-to-back bis(terpyridine) unit amounts to 78.56(6)°.

Py1	N63 C74 C75 C76 C77 C78
Py2	N62 C69 C70 C71 C72 C73
Py3	N61 C64 C65 C66 C67 C68
Py4	N41 C44 C45 C46 C47 C48
Py5	N43 C54 C55 C56 C57 C58
Py6	N42 C49 C50 C51 C52 C53
Py7	N22 C31 C32 C29 C30 C33
Py8	N21 C24 C25 C26 C27 C28
Py9	N23 C34 C35 C36 C37 C38
Py10	N3 C14 C15 C16 C17 C18
Py11	N2 C9 C10 C11 C12 C13
Py12	N1 C4 C5 C6 C7 C8

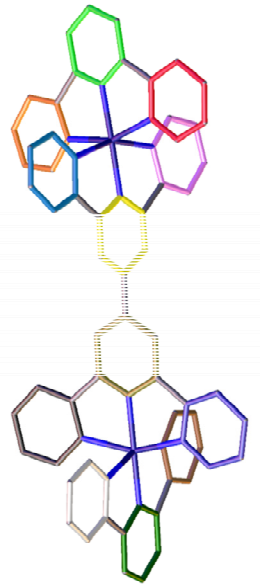

	Py2	Py3	Py4	Py5	Py6	Py7	Py8	Py9	Py10	Py11	Py12
Py1	5.4	7.9	92.1	90.1	90.2	172.9	168.7	169.0	79.4	79.9	83.2
Py2		2.6	87.1	85.5	85.2	167.5	163.8	163.7	74.27	74.7	78.1
Py3			85.1	83.6	83.1	165.0	161.3	161.3	72.0	72.4	75.9
Py4				7.0	2.7	81.3	81.4	77.3	14.6	15.5	10.7
Py5					8.8	83.5	84.4	79.5	17.7	19.2	14.4
Py6						83.0	82.9	79.0	12.1	12.8	8.0
Py7							6.7	4.0	93.6	93.1	89.9
Py8								7.9	92.8	92.0	89.3
Py9									89.7	89.2	85.9
Py10										2.2	4.1
Py11											4.9

The error is typically ±0.1°.

Table S34 Selected bond distances (Å), bond angles (°) in $[Cr_2(tpy)_2(ebbt)](PF_6)_6 \cdot 10CH_3CN$ (**14**).

Bond distances (Å)			
Cr(1)-N(1)	2.063(2)	Cr(1)-N(4)	2.051(2)
Cr(1)-N(2)	1.9871(18)	Cr(1)-N(5)	1.990(2)
Cr(1)-N(3)	2.063(2)	Cr(1)-N(6)	2.069(2)
Bond angles (°)			
N(1)-Cr(1)-N(6)	93.76(9)	N(4)-Cr(1)-N(1)	92.39(9)
N(2)-Cr(1)-N(1)	78.05(8)	N(4)-Cr(1)-N(3)	91.60(9)
N(2)-Cr(1)-N(3)	78.29(8)	N(4)-Cr(1)-N(6)	156.85(9)
N(2)-Cr(1)-N(4)	99.41(8)	N(5)-Cr(1)-N(1)	101.79(8)
N(2)-Cr(1)-N(5)	178.21(9)	N(5)-Cr(1)-N(3)	101.86(8)
N(2)-Cr(1)-N(6)	103.69(8)	N(5)-Cr(1)-N(4)	78.81(9)
N(3)-Cr(1)-N(1)	156.34(8)	N(5)-Cr(1)-N(6)	78.09(9)
N(3)-Cr(1)-N(6)	91.65(9)		

Table S35 Interplanar angles (°) in $[Cr_2(tpy)_2(ebbt)](PF_6)_6 \cdot 10CH_3CN$ (**14**). The interplanar angle between the two chelate CrN_3 planes of the bridging back-to-back bis(terpyridine) unit amounts to 0°.

Py1	N2 C12 C13 C14 C16 C17
Py2	N3 C18 C19 C20 C21 C22
Py3	N1 C7 C8 C9 C10 C11
Py4	N5 C28 C29 C30 C31 C32
Py5	N6 C33 C34 C35 C36 C37
Py6	N4 C23 C24 C25 C26 C27

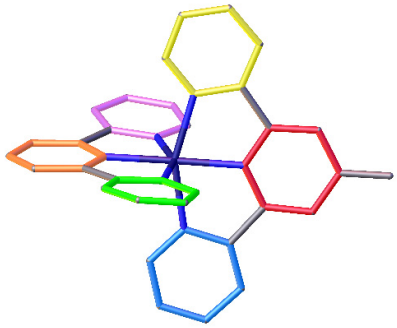

	Py2	Py3	Py4	Py5	Py6
Py1	2.9	2.6	89.2	83.4	93.4
Py2		1.6	91.4	85.6	95.6
Py3			90.0	84.1	94.1
Py4				7.2	6.8
Py5					10.1

The error is typically ±0.1°.

Table S36 Optimized magnetic parameters deduced by means of non-linear least-square fits with eqn (2) of the experimental magnetic susceptibility data collected for the dinuclear chromium complexes.

Compound	J_{ex} /cm^{-1}	g	χ_{dia}^{dimer} /cm^3·mol^{-1}	χ_{TIP}^{dimer} /cm^3·mol^{-1}	Agreement factor [a]
$[Cr_2Cl_6(tppz)]$	-5.4(2)	2.00	$-3.5\cdot10^{-4}$	$2.0\cdot10^{-4}$	$9.6\cdot10^{-3}$
$[Cr_2Cl_6(bbt)]$	-1.36(4)	1.99	$-3.9\cdot10^{-4}$	$7.7\cdot10^{-4}$	$6.8\cdot10^{-3}$
$[Cr_2Cl_6(ebbt)]$	-0.70(2)	1.99	$-4.2\cdot10^{-4}$	$18.8\cdot10^{-4}$	$8.8\cdot10^{-3}$
$[Cr_2(tpy)_2(bbt)](PF_6)_6$	-2.37(4)	1.99	$-9.5\cdot10^{-4}$	$20.3\cdot10^{-4}$	$7.3\cdot10^{-3}$
$[Cr_2(tpy)_2(ebbt)](PF_6)_6$	-2.78(4)	1.99	$-9.6\cdot10^{-4}$	$3.2\cdot10^{-4}$	$3.8\cdot10^{-3}$

[a] Agreement factor: $AF=\sqrt{\sum_T\left(\chi_{exp}T-\chi_{calcd}T\right)^2\Big/\sum_T\left(\chi_{exp}T\right)^2}$

Table S37 $Cr(^2E)$ lifetime, ligand-field energy Δ and Racah parameters (B and C) deduced with eqs (3) and (6) by using the experimental energy of the excited $Cr(^2E)$ and $Cr(^4T_2)$ levels observed for the mononuclear homoleptic $[Cr(L)_2](PF_6)_3$ (L = tpy, ebzpy, ddpd) and heteroleptic $[Cr(L)Cl_3]$ (L = tppz, tpy, ebzpy), $[Cr(ebzpy)(tpy)](PF_6)_3$ and $[Cr(tppz)(tpy)](PF_6)_3$ complexes and assuming $C = 4B$.

Compound	Δ /cm^{-1}	B /cm^{-1}	C /cm^{-1}	Δ/B	E /cm^{-1} [a]					$\tau_{Cr}(^2E)$ /ms	$\tau_{Cr}(^2E)$ /ms
					^2E	$^2T_1$ [b]	$^4T_2$	$^2T_2$ [c]	$^4T_1$ [d]	3K	10 K
$[Cr(tppz)Cl_3]$	16474	693	2770	24	13089	*13846*	16474	*19117*	*23312*	0.24(5)	0.19(5)
$[Cr(tpy)Cl_3]$	16694	697	2786	24	13175	*13931*	16694	*19265*	*23585*	0.85(1)	0.69(1)
$[Cr(ebzpy)Cl_3]$	16287	702	2808	23	13228	*14014*	16287	*19243*	*23169*	1.37(1)	0.27(2)
$[Cr(tpy)_2](PF_6)_3$	18750	675	2698	28	12953	*13584*	18750	*19340*	*25663*	0.56(1)	0.37(1)
$[Cr(ebzpy)_2](PF_6)_3$	18975	689	2754	28	13210	*13860*	18975	*19702*	*26018*	1.24(5)	0.95(5)
$[Cr(ebzpy)(tpy)](PF_6)_3$	19305	651	2605	30	12579	*13150*	19305	*18928*	*26067*	0.33(2)	0.30(2)
$[Cr(tppz)(tpy)](CF_3SO_3)_3$	19120	664	2655	29	12788	*13387*	19120	*19177*	*25974*	0.34(1)	0.27(1)
$[Cr(ddpd)_2](BF_4)_3$[e]	22990	659	2638	35	12903	*13395*	22990	*19752*	*30029*	0.443	

[a] Energies are given with respect to that of the ground $Cr(^4A_2)$ level. [b] Computed with eqn (4). [c] Computed with eqn (7). [d] Computed with eqn (8). [e] The energy of the $Cr(^2E)$ and $Cr(^4A_2)$ levels and $\tau_{Cr}(^2E)$ are taken from reference 120 at 298K.

Table S38 Summary of crystal data, intensity measurements and structure refinements for [Cr(ddpd)Cl_3] (**15**).

	[Cr(ddpd)Cl_3]
Empirical formula	$C_{17}H_{17}Cl_3CrN_5$
Formula weight	449.70 g/mol
Temperature	180.15 K
Radiation (Wavelength)	CuKα (λ = 1.54184)
Crystal System, Space group	monoclinic, $P2_1/n$
Unit cell dimensions	a = 9.2232(4) Å
	b = 14.8231(6) Å
	c = 13.6125(5) Å
	α = 90°
	β = 96.140(4)°
	γ = 90°
Volume in Å^3	1850.38(13)
Z, Calculated density	4, 1.614 g/cm^3
Absorption coefficient	9.171 mm^{-1}
F(000)	916.0
Crystal size (mm^3)	0.343 × 0.179 × 0.125
Theta range for data collection	8.848° to 147.436°
Limiting indices	$-11 \le h \le 11$,
	$-17 \le k \le 17$,
	$-16 \le l \le 16$
Reflections collected	6966
Independent reflections	3620 [R_{int} = 0.0233, R_{sigma} = 0.0310]
Data / restraints / parameters	3620/0/237
Goodness-of-fit on F^2	1.064
Final R indices [$I>2\sigma(I)$]	R_1 = 0.0360, wR_2 = 0.0970
R indices (all data)	R_1 = 0.0410, wR_2 = 0.1018
Largest diff. peak and hole	0.35/-0.43 e.Å^{-3}

Table S39 Selected bond distances (Å), bond angles (°) in [Cr(ddpd)Cl_3] (**15**).

Bond distances (Å)			
Cr(1)-N(1)	2.064(2)	Cr(1)-Cl(1)	2.3413(7)
Cr(1)-N(2)	2.071(2)	Cr(1)-Cl(2)	2.3174(7)
Cr(1)-N(3)	2.071(2)	Cr(1)-Cl(3)	2.3269(7)
Bond angles (°)			
Cl(2)-Cr(1)-Cl(1)	89.25(3)	N(2)-Cr(1)-Cl(1)	90.88(6)
Cl(2)-Cr(1)-Cl(3)	90.01(3)	N(2)-Cr(1)-Cl(2)	178.17(6)
Cl(3)-Cr(1)-Cl(1)	179.11(3)	N(2)-Cr(1)-Cl(3)	89.87(6)
N(1)-Cr(1)-Cl(1)	91.12(6)	N(2)-Cr(1)-N(3)	86.38(8)
N(1)-Cr(1)-Cl(2)	91.63(6)	N(3)-Cr(1)-Cl(1)	87.82(6)
N(1)-Cr(1)-Cl(3)	89.41(6)	N(3)-Cr(1)-Cl(2)	95.45(6)
N(1)-Cr(1)-N(2)	86.54(8)	N(3)-Cr(1)-Cl(3)	91.74(6)
N(1)-Cr(1)-N(3)	172.82(8)		

Table S40 Interplanar angles (°) in [Cr(ddpd)Cl_3] (**15**). The interplanar angle between the chelate CrN_3 plane and the $CrCl_3$ plane amounts to 91.45(4)°.

Py1	N1 C6 C7 C8 C9 C10	
Py2	N2 C12 C13 C14 C15 C16	
Py3	N3 C18 C19 C20 C21 C22	

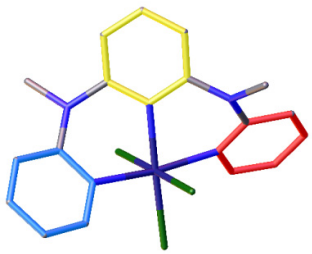

	Py2	Py3
Py1	132.7	106.6
Py2		47.6

The error is typically ±0.1°.

Table S41 Selected FT-IR bands (cm^{-1}) for tpy, $Cr(tpy)Cl_3$, $[Cr(tpy)(CF_3SO_3)_3]$, $[Cr(tpy)_2](CF_3SO_3)_3$.

Compound	ν(C–H)	ν(CC+CN)	δ(C–H)	ν (Cr–N)	ν(Cr–Cl)
tpy	3089w	1580s	800w		
	3049w	1561s	762s		
	3010w	1469s	732s		
		1435s			
		1421s			
		1405sh			
$Cr(tpy)Cl_3$	3076w	1600s	827w	428w	314s
	3062w	1572s	783s	352br395s, s	297sh
	3037w	1560sh	750sh	346sh347sh,s	285sh
		1535w	733m	343s	266w
		1474s			
		1445s			
		1423sh			
		1401m			
$Cr(tpy)(CF_3SO_3)_3$	3108w	1605m	817w	428m	
	3070w	1573w	785br,s	386m	
	3057sh	1541w	771s	357m	
	3040w	1484m	756m	351m	
		1448w	743w		
		1405m	732w		
		1344w			
$[Cr(tpy)_2](PF_6)_3$	3130w	1604s	821s	424m	
	3112w	1572sh	794sh	380w	
		1562w	771s	361m	
		1508w	755sh		
		1481m	740w		
		1448m	729m		
		1406w			
		1371w			

Table S42 Selected FT-IR bands (cm^{-1}) for ebzpy, $Cr(ebzpy)Cl_3$, $[Cr(ebzpy)_2](CF_3SO_3)_3$, $[Cr(ebzpy)_2](PF_6)_3$.

Compound	ν (C–H)	ν (CC+CN)	δ (C–H)	ν (Cr–N)	ν(Cr–Cl)
ebzpy	3084w	1591m	818s		
	3057w	1571s	791m		
		1480w	779w		
		1463m	768m		
		1451m	750s		
		1435s			
		1415s			
		1392w			
$Cr(ebzpy)Cl_3$	3100w	1600m	806br	395s	284w
	3068w	1591sh	791w	361s	270w
	3035w	1567w	768s	339sh,s	
		1522sh	756s	332br,s	
		1514m	735br,s		
		1481s			
		1460m			
		1443s			
		1385m			
$[Cr(ebzpy)_2](CF_3SO_3)_3$	3103w	1601m	814w	428s	
	3070sh	1562w	790w	357br,s	
		1526m	748-734br,s	338sh	
		1489s			
		1468s			
		1443s			
		1385w			
$[Cr(ebzpy)_2](PF_6)_3$	3130w	1602m	817w	357s	
	3083w	1595sh	788sh	340sh	
		1564w	775s		
		1527m	756w		
		1487s	746w		
		1468s	735sh		
		1442s			
		1385m			

Table S43 Selected FT-IR bands (cm^{-1}) for tppz, $Cr(tppz)Cl_3$, $Cr(tppz)(CF_3SO_3)_3$, $[Cr(tppz)(tpy)](CF_3SO_3)_3$.

Compound	ν(C–H)	ν(CC+CN)	δ (C–H)	ν(Cr–N)	ν(Cr–Cl)
tppz	3078w	1587s	807s	–	–
	3050w	1566s	782s		
	3015w	1486w	752m		
		1476m			
		1435m			
		1391s			
$Cr(tppz)Cl_3$	3098w	1598m	816s	393s	322m
	3070w	1580m	800s	352br,s	279w
	3040w	1564w	770s	346sh	
		1534w	754s		
		1476m	734w		
		1460w			
		1447w			
		1404s			
		1389m			
$Cr(tppz)(CF_3SO_3)_3$	3106w	1603w	810m	381s	
	3070w	1540m	783s	354w	
	3060w	1477sh	771m	345br	
		1466m	759sh		
		1431m	746m		
		1410sh			
		1390w			
$[Cr(tppz)(tpy)](CF_3SO_3)_3$	3091w	1604m	817w	403 m	
	3070w	1589sh	788sh	360w	
		1571w	775s	347m	
		1535w	756w		
		1483w	746w		
		1469sh	735sh		
		1450m			
		1403m			
		1392sh			

Table S44 Selected FT-IR bands (cm^{-1}) for $[Cr(tpy)(ebzpy)](PF_6)_3$.

Compound	ν(C–H)	ν(CC+CN)	δ(C–H)	ν(Cr–N)	ν(Cr–Cl)
$[Cr(tpy)(ebzpy)](PF_6)_3$	3114w	1603m	820s	406sh	
	3015w	1593sh	789w	363br,w	
		1573sh	775s	355br,w	
		1564w	753w	349br,w	
		1531w	739m		
		1508w	731sh		
		1490br,m			
		1479br,m			
		1471br,m			
		1447m			
		1404w			
		1390w			

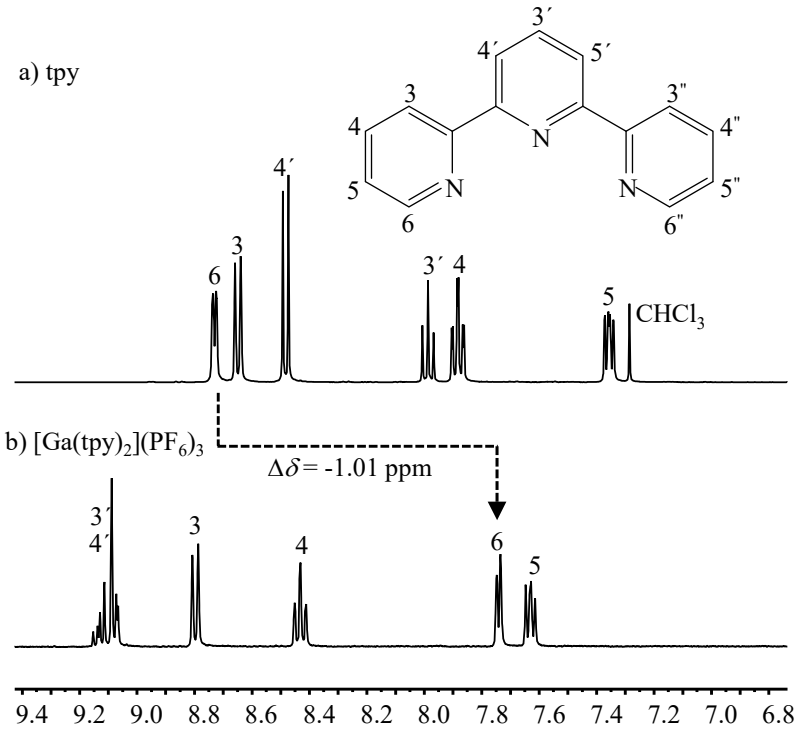

Fig. S1 ^{1}H NMR spectrum of a) tpy ($CDCl_3$, 295 K) and b) $[Ga(tpy)_2](PF_6)_3$ with numbering scheme (CD_3CN, 5 mM, 295 K).

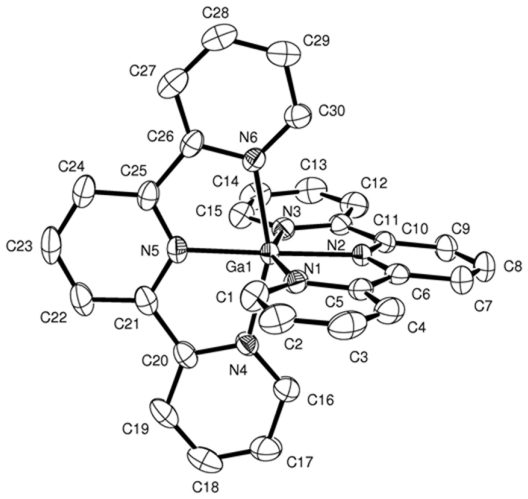

Fig. S2 Ortep view of $[Ga(tpy)_2](PF_6)_3 \cdot 2CH_3CN$ (**1**) with numbering scheme. Thermal ellipsoids are drawn at 50% probability level. Counter ions, solvent molecules and H atoms are omitted for clarity.

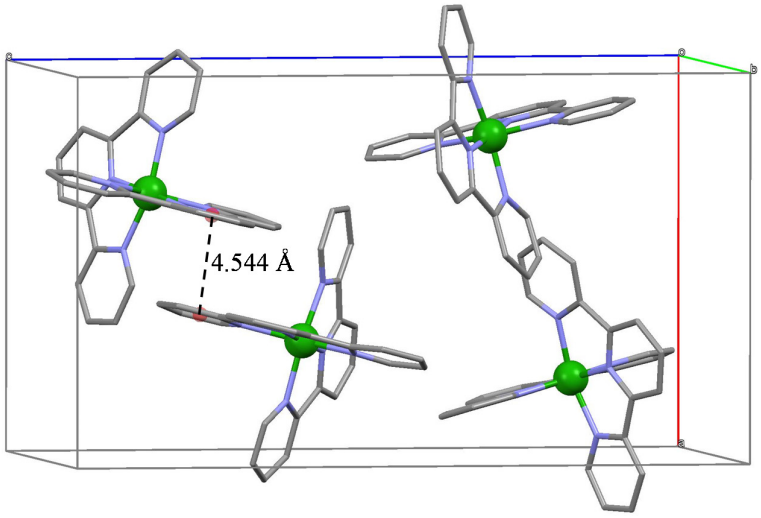

Fig. S3 Shortest intermolecular aromatic stacking distances observed in the crystal structure of $[Ga(tpy)_2](PF_6)_3 \cdot 2CH_3CN$ (**1**).

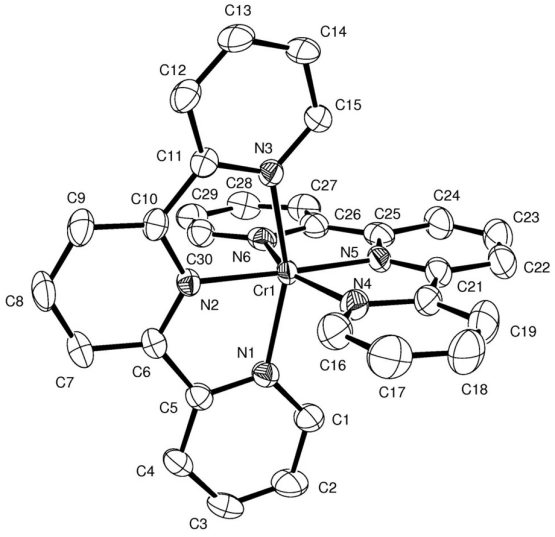

Fig. S4 Ortep view of $[Cr(tpy)_2](PF_6)_3 \cdot 2.5CH_3CN$ (**2**) with numbering scheme for one of the four independent complexes. Thermal ellipsoids are drawn at 40% probability level. Counter ions, solvent molecules and H atoms are omitted for clarity.

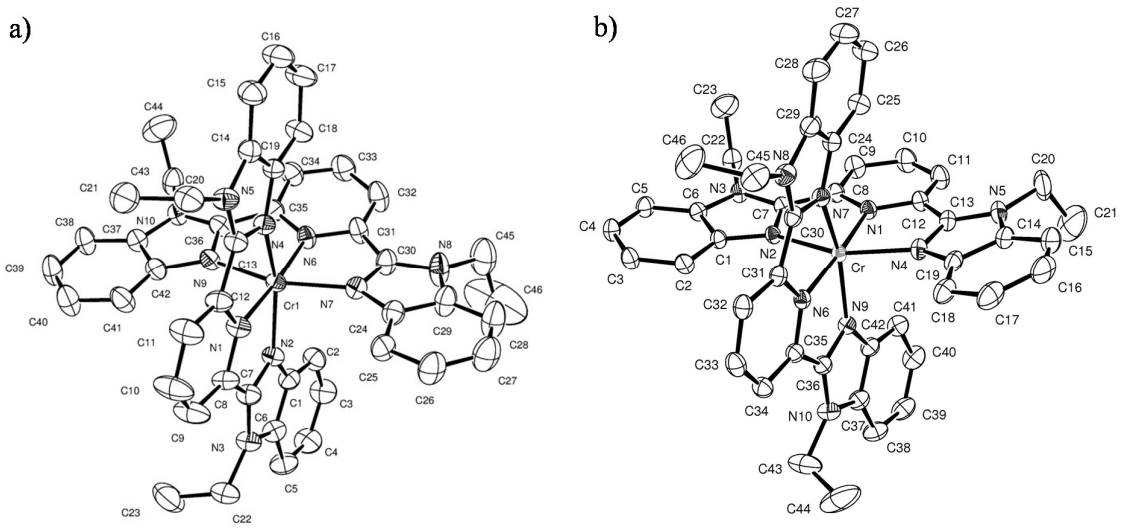

Fig. S5 Ortep views of a) $[Cr(ebzpy)_2](PF_6)_3 \cdot 5.5CH_3CN$ (one of the two independent complexes) (**3**) and b) $[Cr(ebzpy)_2](CF_3SO_3)_3 \cdot 2CH_3CN$ (**4**) with numbering scheme. Thermal ellipsoids are drawn at 40% probability level. Counter ions, solvent molecules and H atoms are omitted for clarity.

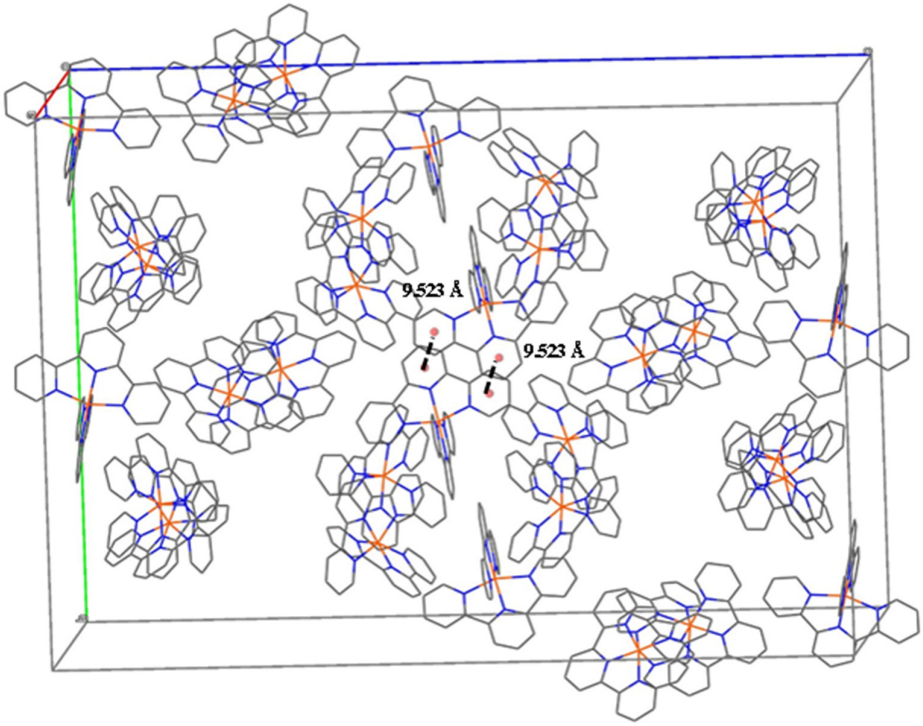

Fig. S6 Shortest intermolecular aromatic stacking distances observed in the crystal structure of $[Cr(tpy)_2](PF_6)_3 \cdot 2.5CH_3CN$ (**2**).

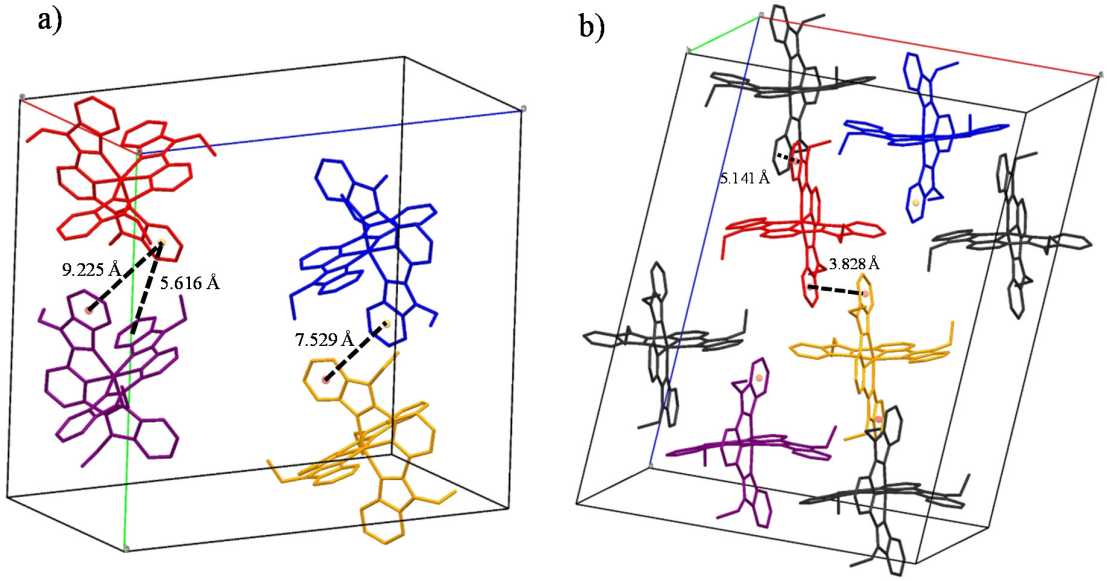

Fig. S7 Shortest intermolecular aromatic stacking distances observed in the crystal structure of a) $[Cr(ebzpy)_2](PF_6)_3 \cdot 5.5CH_3CN$ (**3**) and b) $[Cr(ebzpy)_2](CF_3SO_3)_3 \cdot 2CH_3CN$ (**4**).

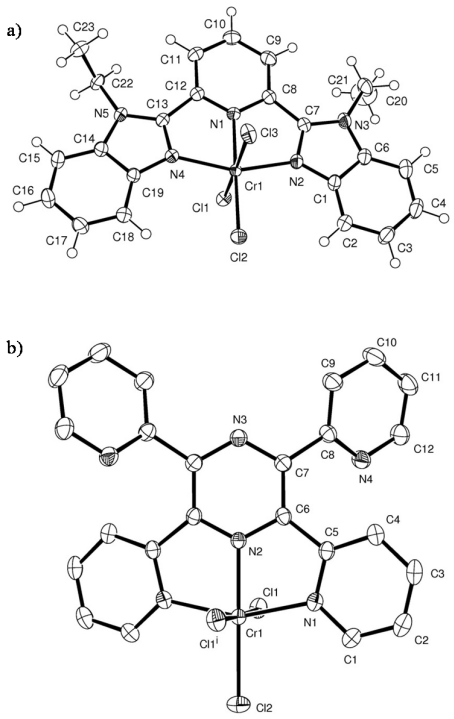

Fig. S8 Ortep views of a) [Cr(ebzpy)Cl_3]·DMF (**5**) and [Cr(tppz)Cl_3]·2DMF (**6**) with numbering scheme. Thermal ellipsoids are drawn at 50% probability level. Solvent molecules and H atoms are omitted for clarity.

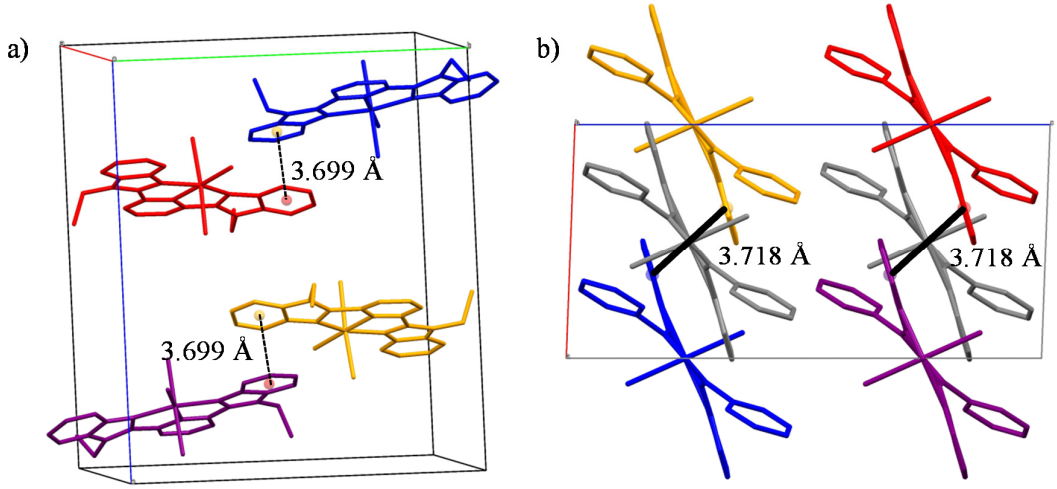

Fig. S9 Intermolecular π-stacking distances found in a) [Cr(ebzpy)Cl_3]·DMF (**5**) where each complex is involved in two intermolecular benzimidazole···benzimidazole interactions (d = 3.699 Å, angle 12.76°) with neighboring molecules related by inversion centers and b) [Cr(tppz)Cl_3]·2DMF (**6**), where the central pyrazine groups display two intermolecular pyridine ···pyridine interactions (d = 3.718 Å, angle = 0.54°).

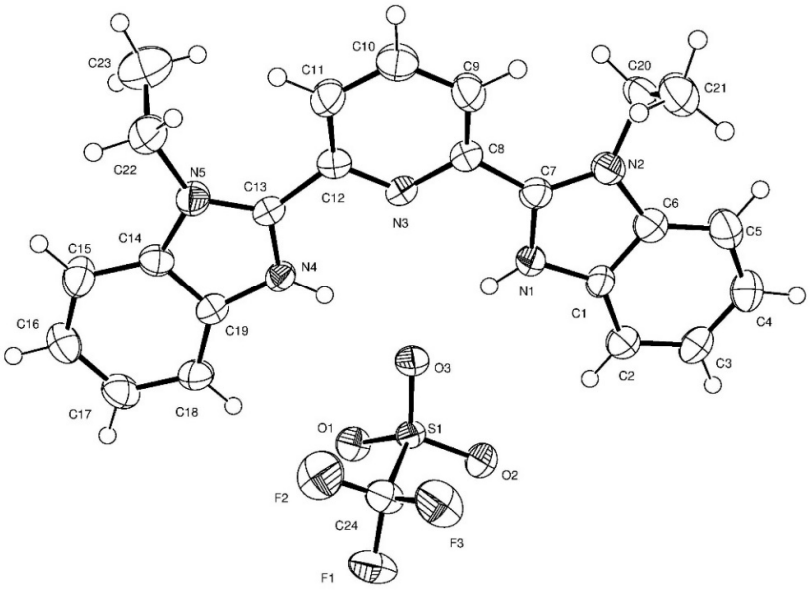

Fig. S10 Ortep view of $[H_2(ebzpy)](CF_3SO_3)_2$ (**10**) with numbering scheme. Thermal ellipsoids are drawn at 50% probability level. The ionic triflate counter anion is omitted for clarity.

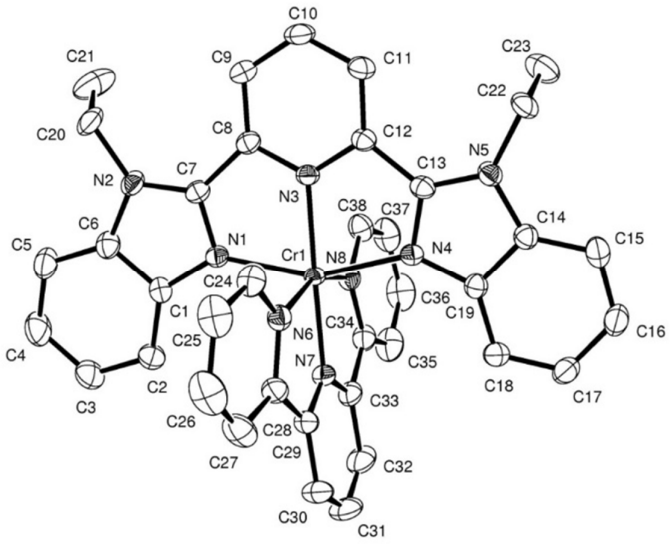

Fig. S11 Ortep view of $[Cr(tpy)(ebzpy)](PF_6)_3 \cdot 2CH_3CN$ (**7**) with numbering scheme. Thermal ellipsoids are drawn at 50% probability level. Counter ions and solvent molecules are omitted for clarity.

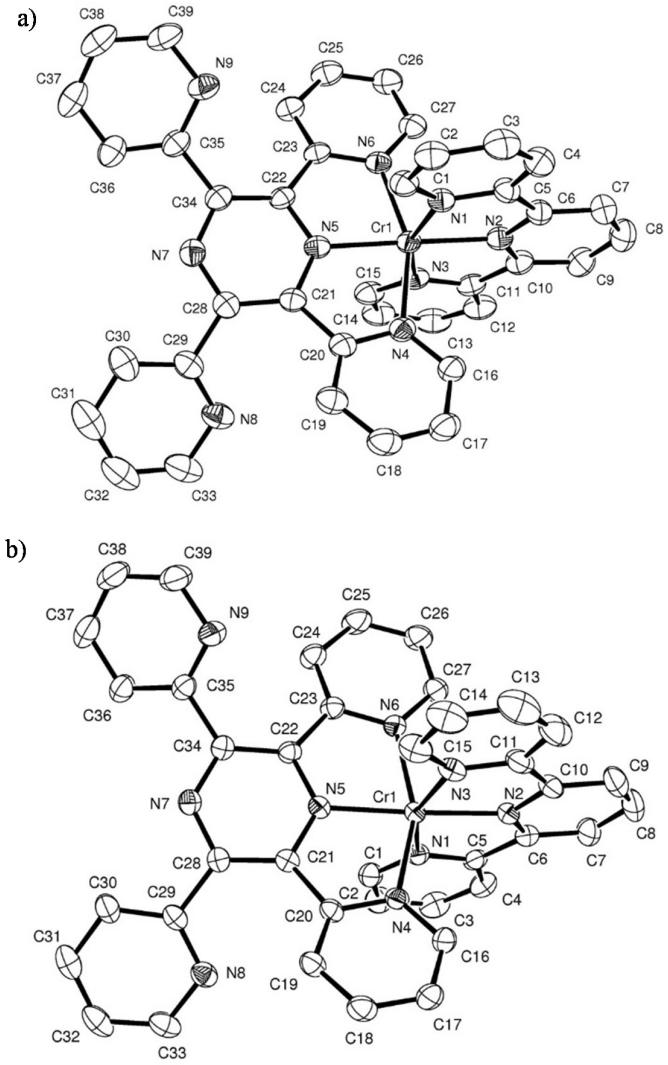

Fig. S12 Ortep views of a) $[Cr(tpy)(tppz)](PF_6)_3 \cdot 3CH_3CN$ (**8**) and b) $[Cr(tpy)(tppz)](CF_3SO_3)_3 \cdot CH_3CN$ (**9**) with numbering scheme. Thermal ellipsoids are drawn at 40% probability level. Counter ions, solvent molecules and H atoms are omitted for clarity.

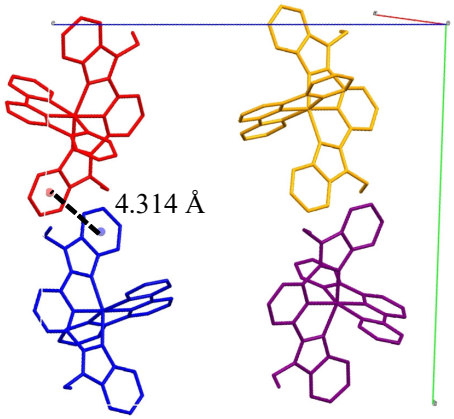

Fig. S13 Intermolecular π-stacking interactions found in $[Cr(tpy)(ebzpy)](PF_6)_3 \cdot 2CH_3CN$ (**7**). The solvents molecules and counter ions are omitted for clarity.

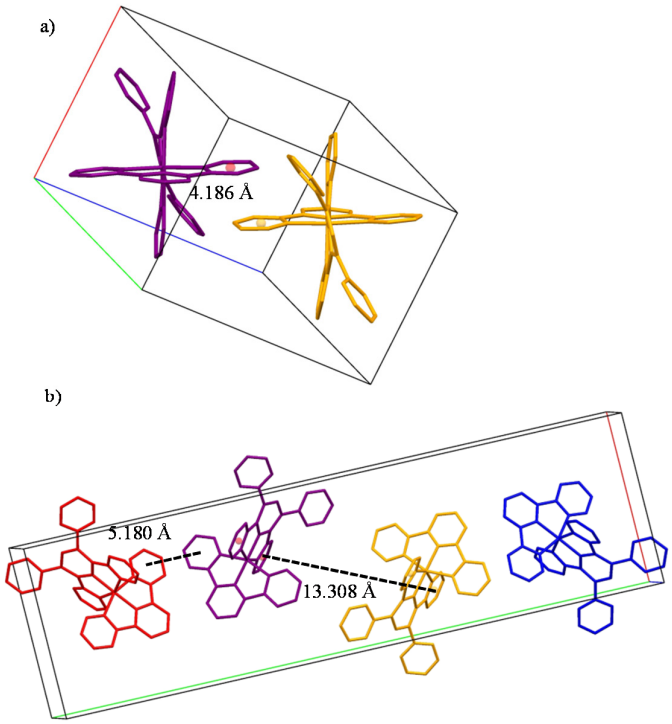

Fig. S14 Intermolecular π-stacking distances found in a) $[Cr(tpy)(tppz)](PF_6)_3 \cdot 3CH_3CN$ (**8**) and b) $[Cr(tpy)(tppz)](CF_3SO_3)_3 \cdot CH_3CN$ (**9**). The solvents molecules and counter ions are omitted for clarity.

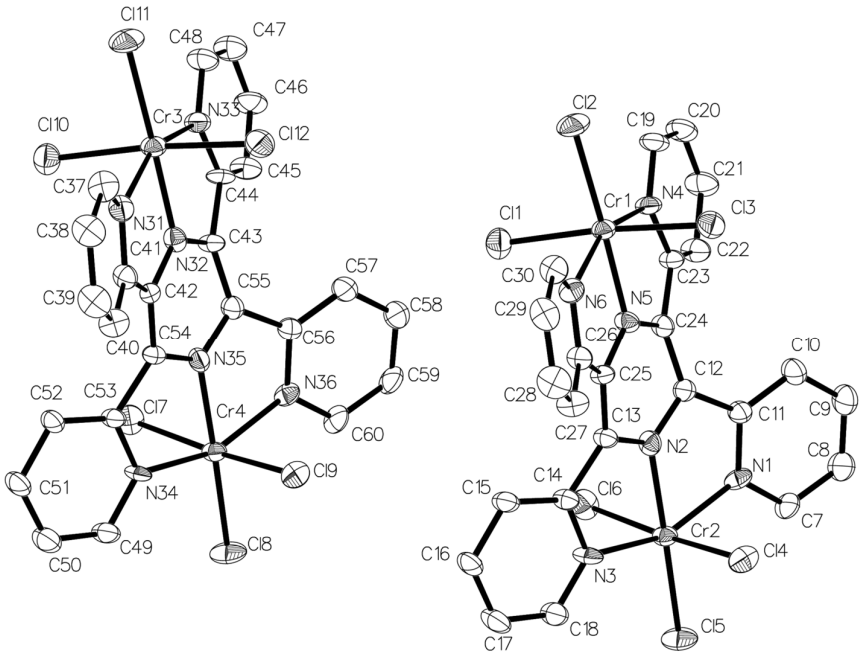

Fig. S15 Ortep views of the two different complexes in the asymmetric unit of $[Cr_2Cl_6(tppz)]\cdot 3C_5H_9NO$ (**11**) with numbering scheme. Thermal ellipsoids are drawn at 50% probability level. Counter ions, solvent molecules and H atoms are omitted for clarity.

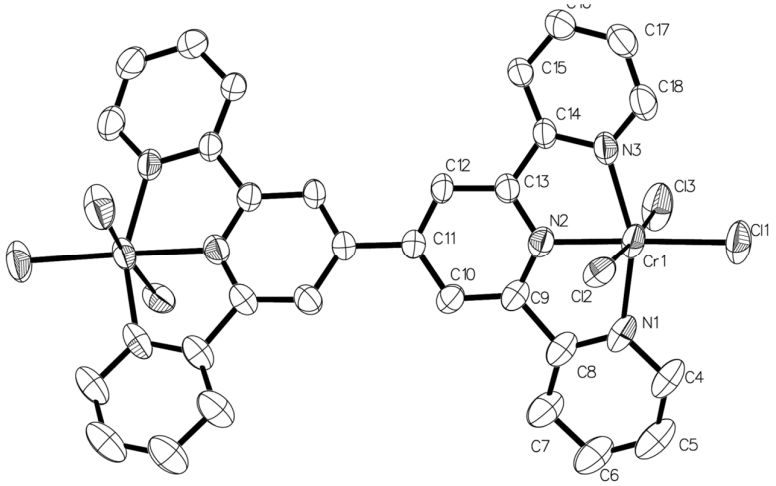

Fig. S16 Ortep views of $[Cr_2Cl_6(bbt)]$ (**12**) with numbering scheme. Thermal ellipsoids are drawn at 50% probability level. Counter ions, solvent molecules and H atoms are omitted for clarity.

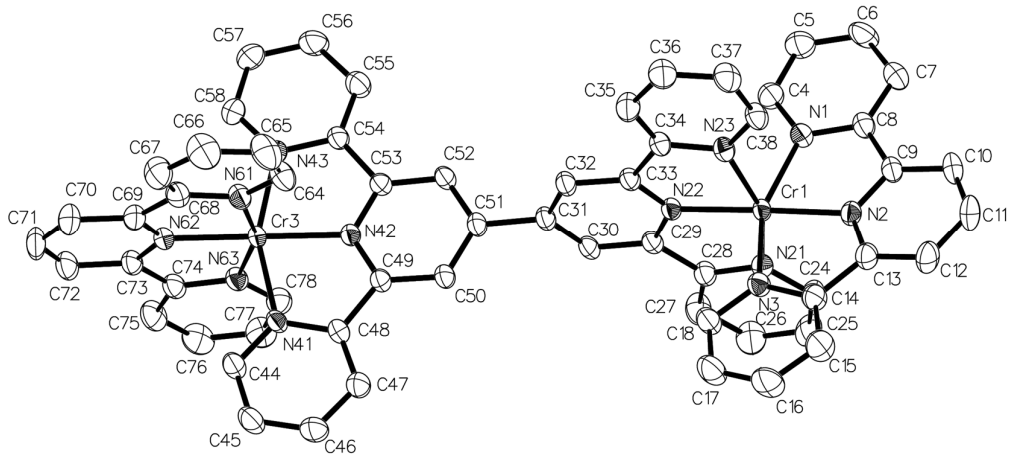

Fig. S17 Ortep views of $[Cr_2(tpy)_2(bbt)](PF_6)_6 \cdot 8CH_3CN \cdot (CH_3CH_2)_2O$ (**13**) with numbering scheme. Thermal ellipsoids are drawn at 50% probability level. Counter ions, solvent molecules and H atoms are omitted for clarity.

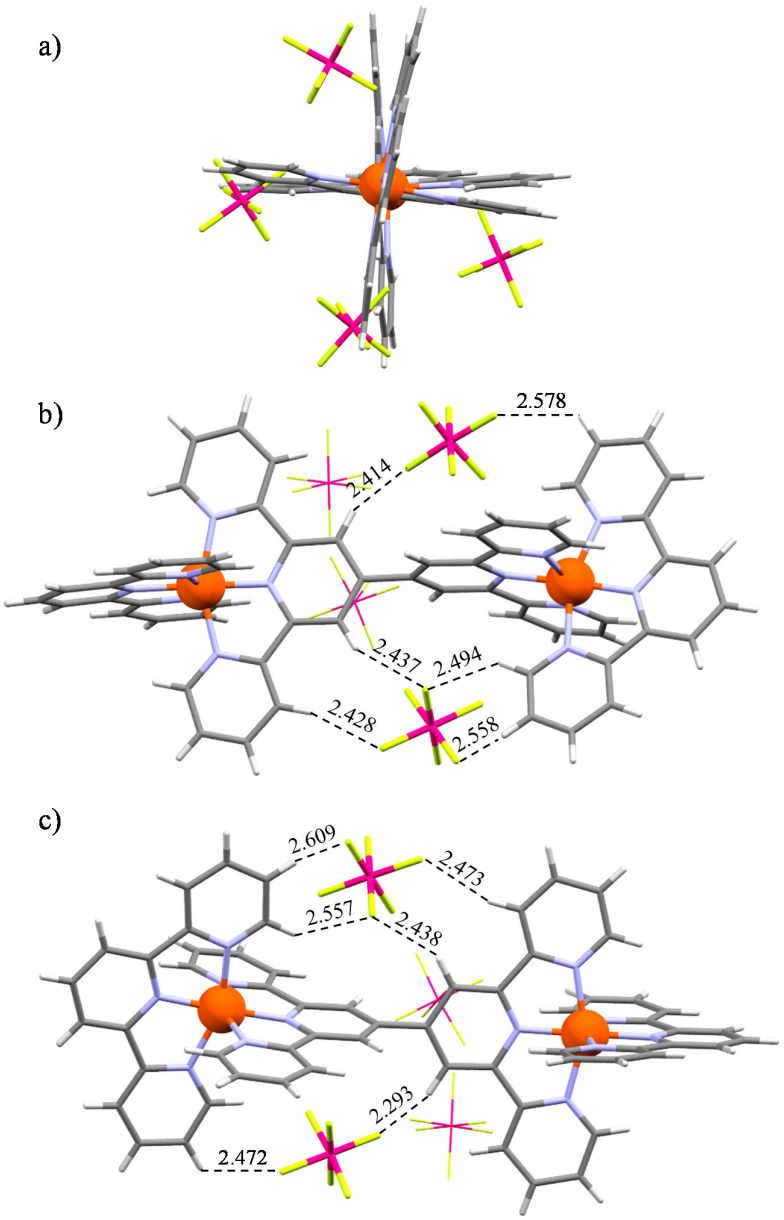

Fig. S18 Perspective views of the crystal structure of $[Cr_2(tpy)_2(bbt)](PF_6)_6 \cdot 8CH_3CN \cdot (CH_3CH_2)_2O$ (**13**) showing a) the $[Cr_2(tpy)_2(bbt)]^{6+}$ and the four PF_6^- anions involved in C-H···F intermolecular bonding network and b) and c) the twelve internuclear C-H···F distances. Color codes: C = grey, N = blue, Cr = orange, H = white, P = magenta, F = yellow.

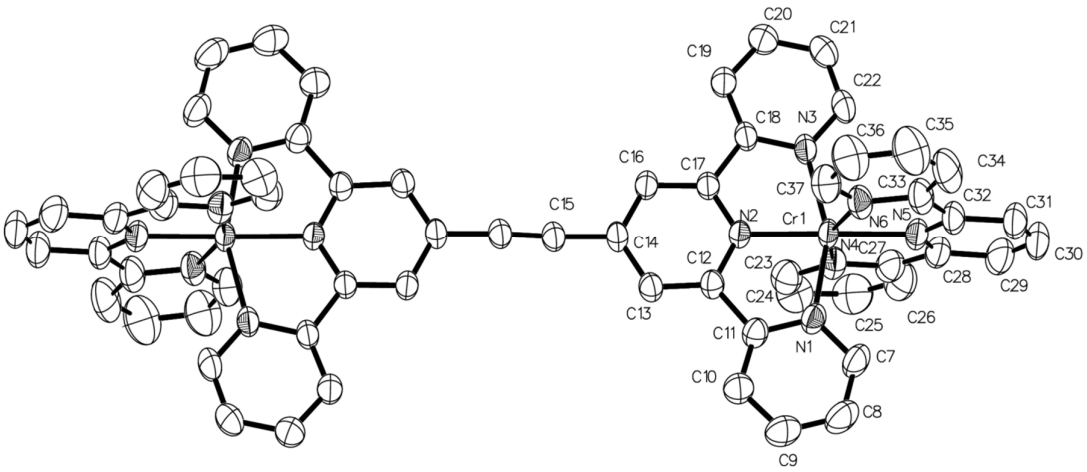

Fig. S19 Ortep views of $[Cr_2(tpy)_2(ebbt)](PF_6)_6 \cdot 10CH_3CN$ (**14**) with numbering scheme. Thermal ellipsoids are drawn at 50% probability level. Counter ions, solvent molecules and H atoms are omitted for clarity.

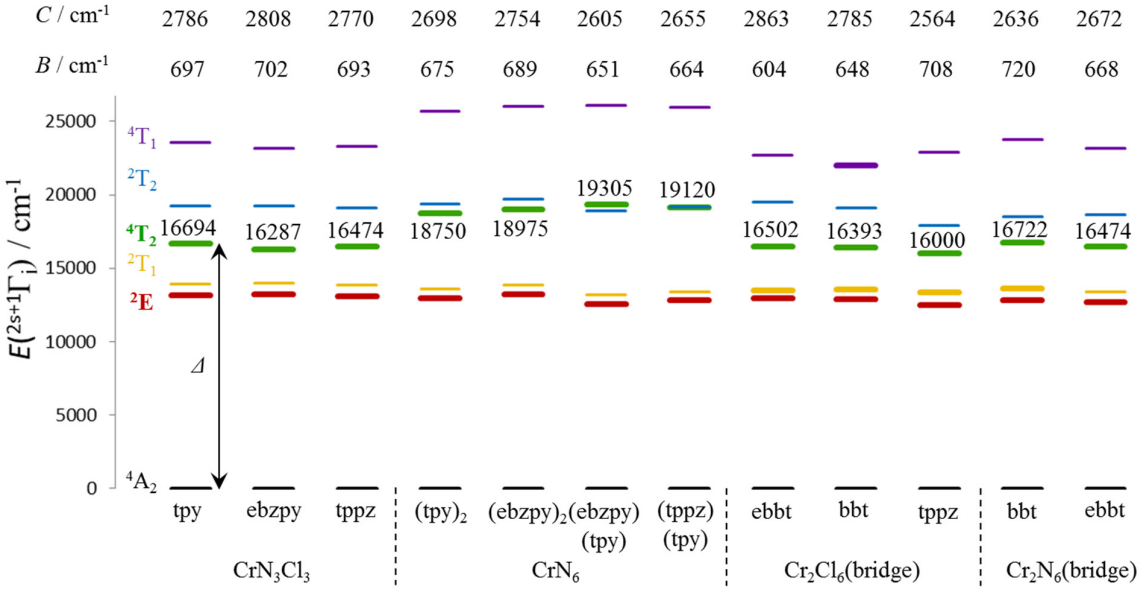

Fig. S20 Low-energy part of the Dieke diagrams obtained for the dinuclear $[Cl_3Cr(L)CrCl_3]$ and $[(tpy)Cr(L)Cr(tpy)](PF_6)_6$ (L = tppz, bbt, ebbt) and the mononuclear $[Cr(L)Cl_3]$ (L = ebzpy, tppz, tpy), $[Cr(L)_2](PF_6)_3$ (L = tpy, ebzpy), $[Cr(tpy)(ebzpy)](PF_6)_3$ and $[Cr(tpy)(tppz)](PF_6)_3$ chromium complexes. The ligand-field and Racah parameters are highlighted. Bold traces are used for experimentally observed excited levels, whereas thin traces correspond to calculated levels.

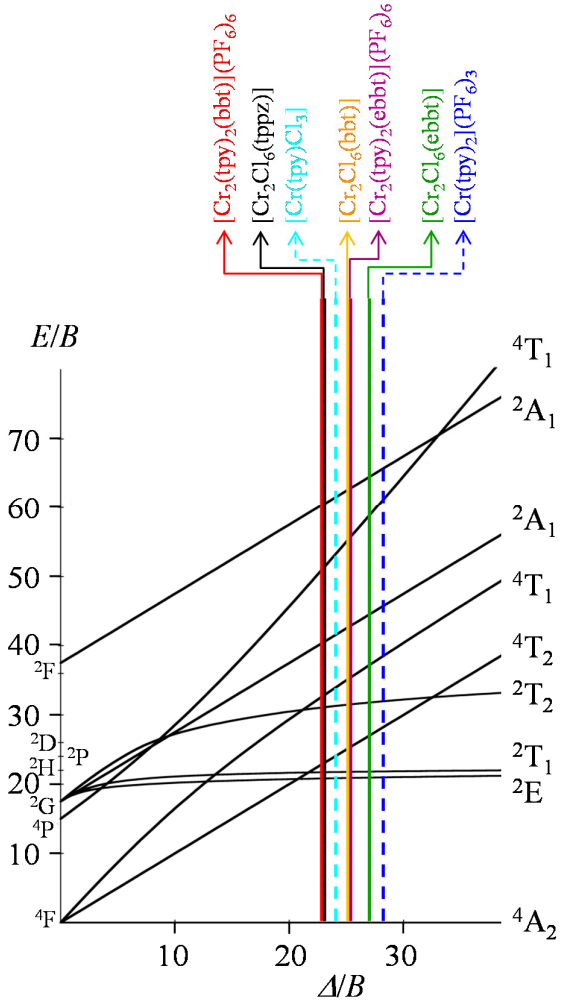

Fig. S21 Low-energy part of the energy level diagram (Tanabe-Sugano) for d^3 ions in an octahedral field (C/B = 4) showing the Δ/B ratios found for the dimeric $[Cl_3Cr(L)CrCl_3]$ and $[(tpy)Cr(L)Cr(tpy)](PF_6)_6$ complexes (L = ttpz, bbt, ebbt) and for their mononuclear analogues $[(tppz)CrCl_3]$, $[(tpy)CrCl_3]$ and $[Cr(tpy)_2](PF_6)_3$.

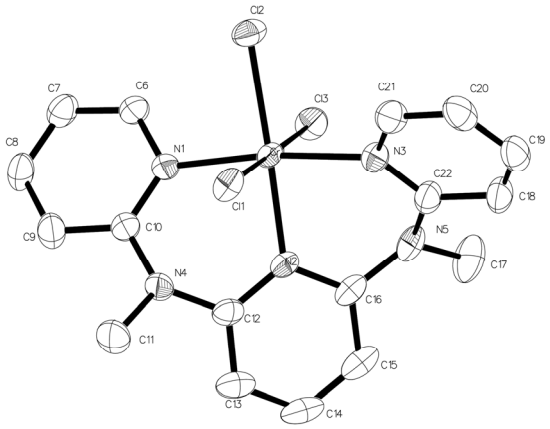

Fig. S22 Ortep view of [Cr(ddpd)Cl_3] (**15**) with numbering scheme. Thermal ellipsoids are drawn at 50% probability level. Counter ions, solvent molecules and H atoms are omitted for clarity.

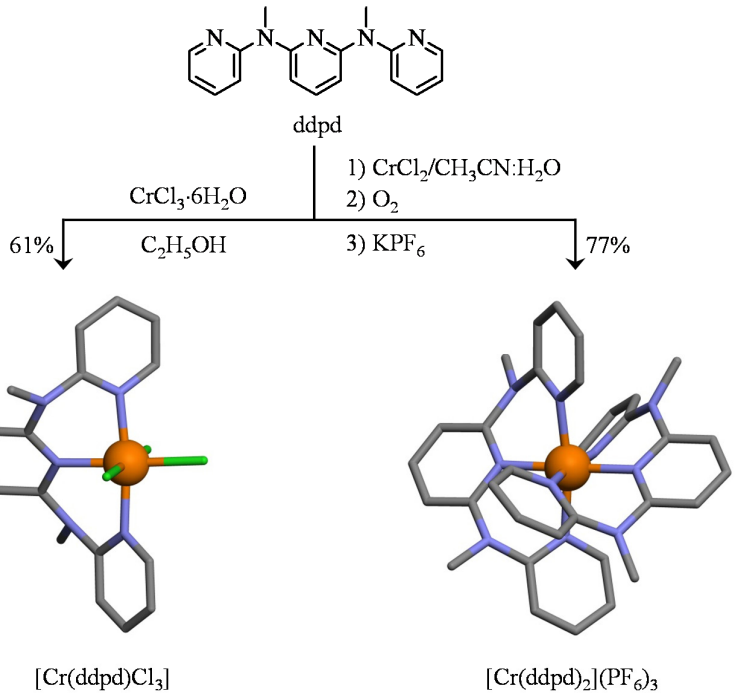

Fig. S23 Synthesis of mononuclear chromium complexes six-membered chelate rings. The molecular structures are those found in the crystal structures of [Cr(ddpd)Cl_3] (**15**) and [Cr(ddpd)$_2$](PF_6)$_3$·CH_3CN.[120] The hydrogen atoms have been omitted for clarity. Color code: C = grey, N = blue, Cr = orange, Cl = green.

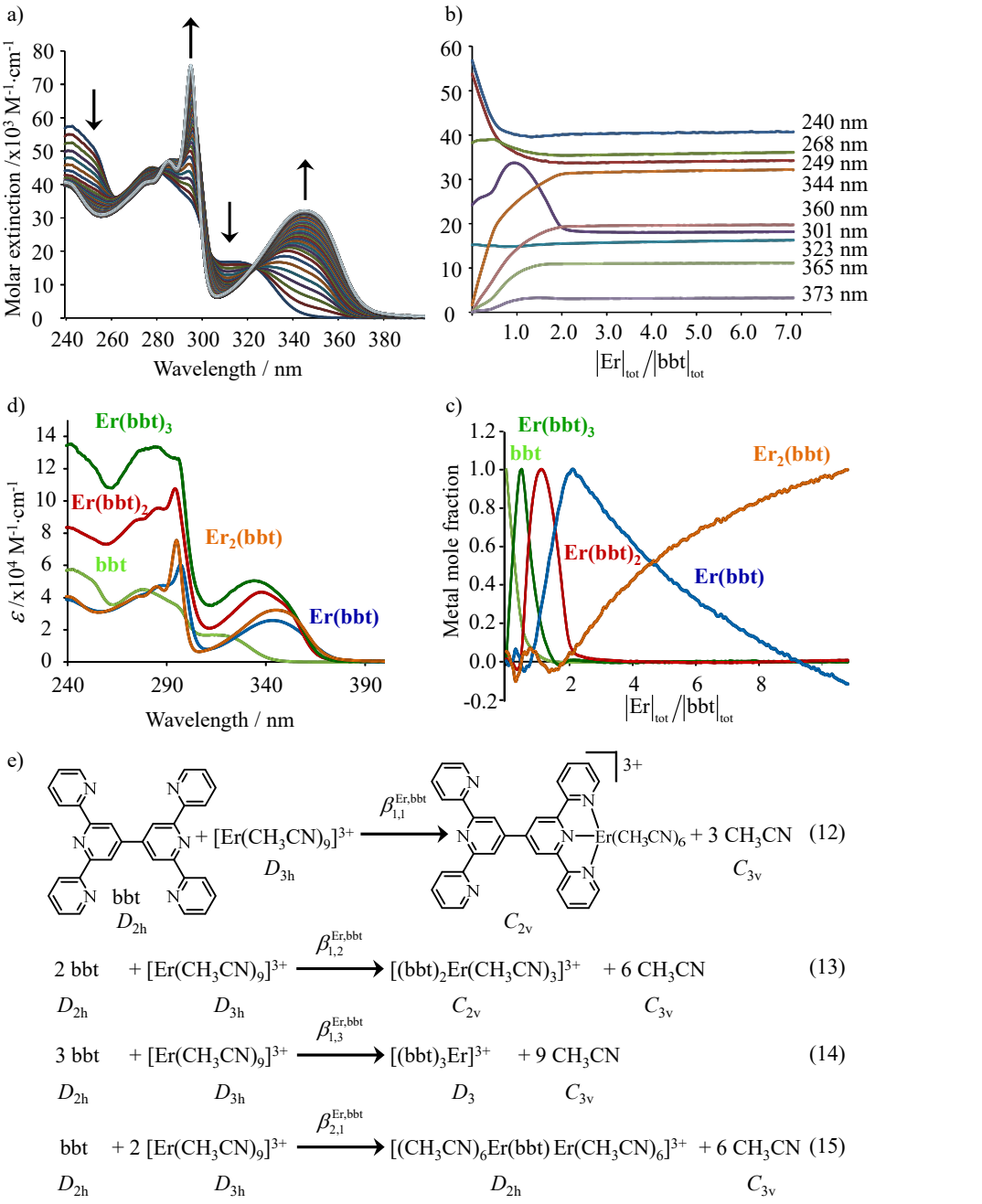

Fig. S24 a) Variation of absorption spectra and b) corresponding variation of observed molar extinctions at different wavelengths observed for the spectrophotometric titration of bbt with $Er(CF_3SO_3)_3$ (total ligand concentration: $9 \cdot 10^{-5}$ mol·dm^{-3} in CH_3CN:$CHCl_3$ = 65:35, 298K). c) Evolving factor analysis using five absorbing eigenvectors,[130] d) re-constructed individual electronic absorption spectra[131] and e) proposed thermodynamic model.

Appendix 1: Absorption data

Table A1-1 Electronic absorption spectra for mononuclear homoleptic and heteroleptic Cr^{III} complexes in solution at 293 K.

Compound	Solvent	λ (nm)	$\bar{\upsilon}$ (cm^{-1})	ε ($M^{-1}.cm^{-1}$)	Assignment
$[Cr(tpy)Cl_3]$	DMF	288^{sh}	34722	12050	$\pi\rightarrow\pi^*$
		321	31153	12400	
		335	29850	16400	
		360	27778	2300	
		391	25575	400	LMCT
		414	24155	200	
		448	22321	150	
		599	16694	150	Cr ($^4T_2 \leftarrow {}^4A_2$)
$[Cr(ebzpy)Cl_3]$	DMF	293^{sh}	34130	17100	$\pi\rightarrow\pi^*$
		326	30675	27500	
		355^{sh}	28169	20600	
		386	25907	11000	
		614	16287	100	Cr ($^4T_2 \leftarrow {}^4A_2$)
$[Cr(tppz)Cl_3]$	DMF	297	33670	22062	$\pi\rightarrow\pi^*$
		354	28249	22870	
		607	16474	150	Cr ($^4T_2 \leftarrow {}^4A_2$)
$[Cr(tpy)_2](PF_6)_3$	CH_3CN	277	36101	30600	$\pi\rightarrow\pi^*$
		316	31646	13200	
		352	28409	15000	
		368	27174	15900	
		422	23697	2000	LMCT
		446	22422	2050	
		476^{sh}	21008	1300	
		533^{sh}	18750	125	Cr ($^4T_2 \leftarrow {}^4A_2$)
$[Cr(ebzpy)_2](PF_6)_3$[(a)]	CH_3CN	314	31847	48200	$\pi\rightarrow\pi^*$
		363	27548	26250	
		438	22831	6550	LMCT
		488^{sh}	20492	2700	
		527^{sh}	18975	1500	Cr ($^4T_2 \leftarrow {}^4A_2$)
$[Cr(ebzpy)(tpy)](PF_6)_3$	CH_3CN	291	34364	29900	$\pi\rightarrow\pi^*$
		320	31250	32550	
		359^{sh}	27855	19200	
		427^{sh}	23419	4450	LMCT
		475^{sh}	21053	1850	
		518	19305	850	Cr ($^4T_2 \leftarrow {}^4A_2$)
$[Cr(tppz)(tpy)](CF_3SO_3)_3$	CH_3CN	222^{sh}	45045	57278	$\pi\rightarrow\pi^*$
		259^{sh}	38610	29856	
		291	34364	27029	
		326^{sh}	30675	25002	
		348	28736	23476	
		365^{sh}	27397	20390	
		401^{sh}	24938	13158	LMCT
		476	21008	1427	
		523	19120	856	Cr ($^4T_2 \leftarrow {}^4A_2$)

Energies are given for the maximum of the band envelope in cm^{-1} . sh = shoulder,

Table A1-2 Electronic absorption spectra for dinuclear Cr^{III} complexes in acetonitrile, in *N*-methyl-pyrrolidone (NMP) or in the solid state (SS) at 293 K.

Compound	Solvent	λ (nm)	$\bar{\upsilon}$ (cm^{-1})	ε ($M^{-1}.cm^{-1}$)	Assignment
		306	32616	12543	π→π*
		395	25291	14358	
		483	20687	1482	LMCT
$[Cr_2Cl_6(tppz)]$	NMP	625	16108	130	Cr ($^4T_2 \leftarrow {}^4A_2$)
		751[c]	13316		Cr ($^2T_1 \leftarrow {}^4A_2$)
		300	33333	39420	π→π*
		332	30120	18300	
		346	28902	20490	
		397	25189	1610	LMCT
$[Cr_2Cl_6(bbt)]$	NMP	455	21978	244	Cr ($^4T_1 \leftarrow {}^4A_2$)
		610	16393	211	Cr ($^4T_2 \leftarrow {}^4A_2$)
		737[c]	13569		Cr ($^2T_1 \leftarrow {}^4A_2$)
		761[c]	13141		Cr ($^2E \leftarrow {}^4A_2$)
		260[c]	38462		π→π*
		350[c]	28571		
$[Cr_2Cl_6(ebbt)]$	SS	606[c]	16502		Cr ($^4T_2 \leftarrow {}^4A_2$)
		741[c]	13495		Cr ($^2T_1 \leftarrow {}^4A_2$)
		292	34247	175000	π→π*
		352	28409	76169	
		365	27397	84773	
		446	22422	10730	LMCT
$[Cr_2(tpy)_2(bbt)](PF_6)_6$	CH_3CN	477	20964	7091	
		598	16722	217	Cr ($^4T_2 \leftarrow {}^4A_2$)
		734	13624	29	Cr ($^2T_1 \leftarrow {}^4A_2$)
		775[c]	12903		Cr ($^2E \leftarrow {}^4A_2$)
		206	48544	129000	π→π*
		224	44643	106000	
		290	34483	56986	
$[Cr_2(tpy)_2(ebbt)](PF_6)_6$	CH_3CN	353	28329	62362	
		450	22222	4771	LMCT
		476	21008	3121	
		607	16474	72	Cr ($^4T_2 \leftarrow {}^4A_2$)

Energies are given for the maximum of the band envelope in cm^{-1}. [c]Transitions observed in the solid state.

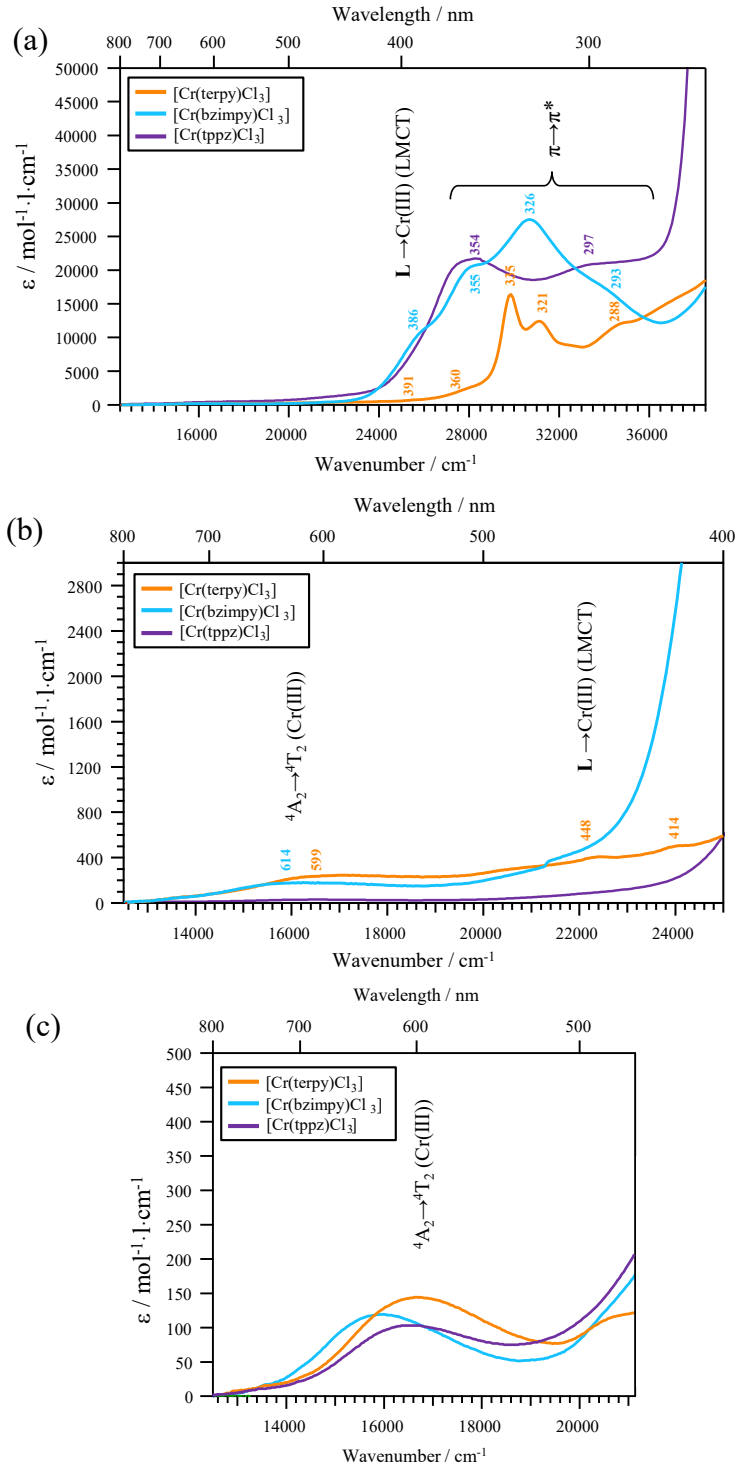

Fig. A1-1 Absorption spectra of [Cr(tpy)Cl3], [Cr(ebzpy)Cl3] and [Cr(tppz)Cl3] complexes in dimethylformamide (DMF) at room-temperature. (a,b) C = 3.67-4.10·10^{-4} mol·L^{-1} and (c) C = 1.43-1.61·10^{-3} mol·L^{-1}.

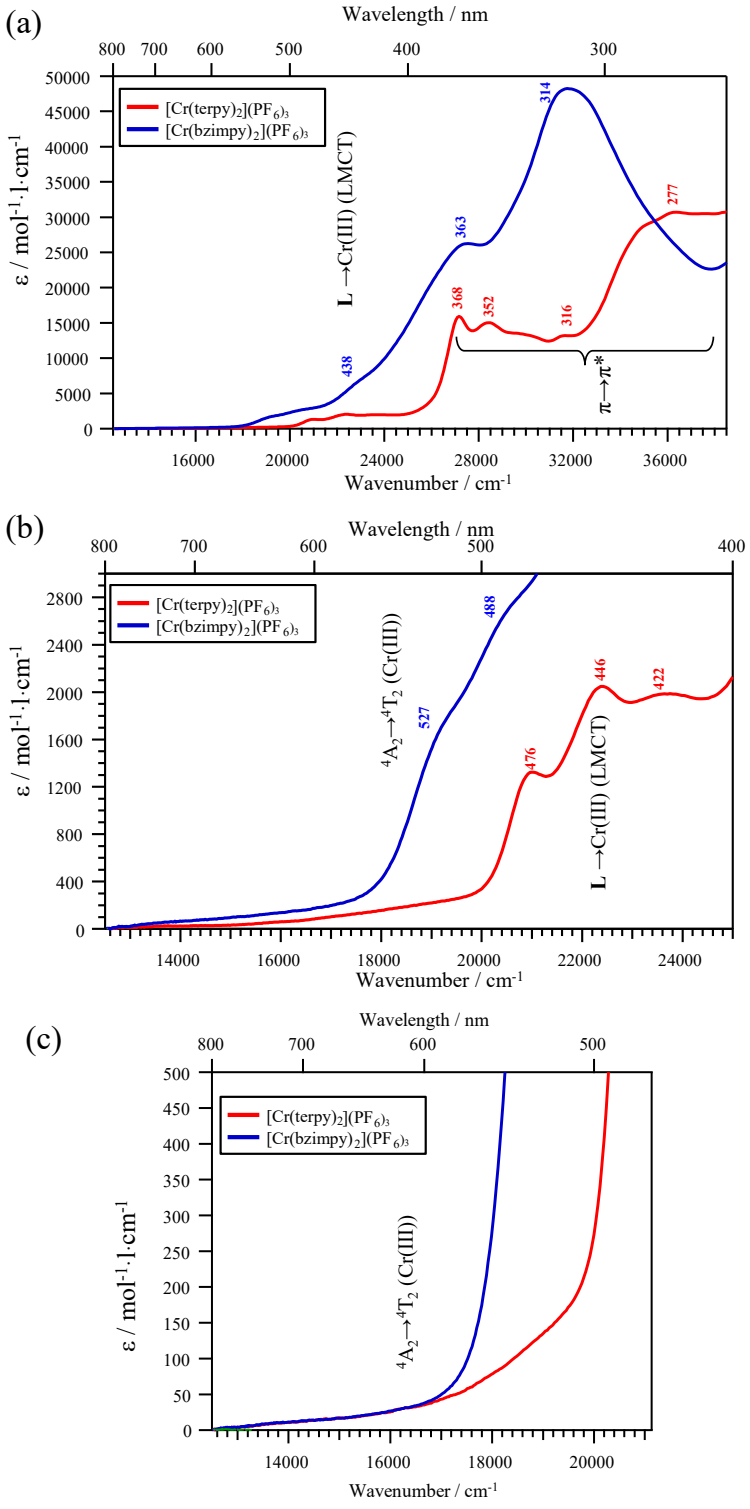

Fig. A1-2 Absorption spectra of homoleptic $[Cr(tpy)_2](PF_6)_3$ and $[Cr(ebzpy)_2](PF_6)_3$, complexes in acetonitrile at room-temperature. (a,b) $C = 3.67\text{-}4.10 \cdot 10^{-4}$ mol·L^{-1} and (c) $C = 1.43\text{-}1.61 \cdot 10^{-3}$ mol·L^{-1}.

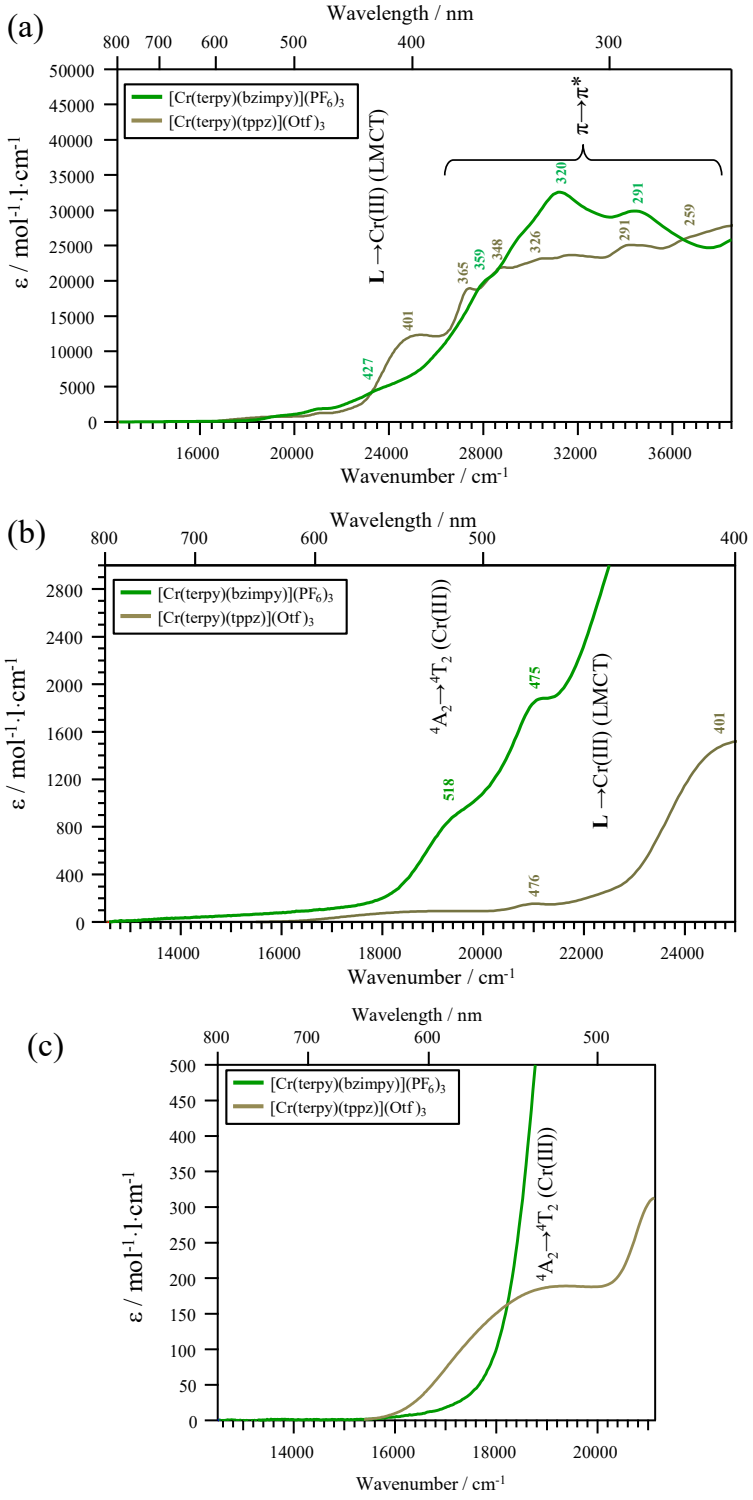

Fig. A1-3 Absorption spectra of the heteroleptic $[Cr(tpy)(ebzpy)](PF_6)_3$ and$[Cr(tpy)(tppz)](PF_6)_3$ complexes in acetonitrile at room-temperature. (a,b) C = 3.67-4.10·10^{-4} mol·L^{-1} and (c) C = 1.43-1.61·10^{-3} mol·L^{-1}.

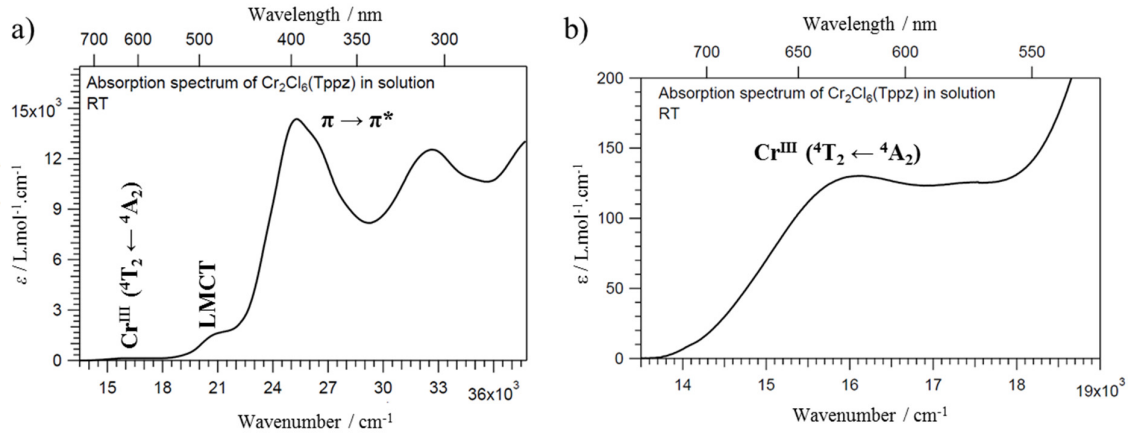

Fig. A1-4 Absorption spectrum of the bimetalic Cr_2Cl_6(tppz) complex in NMP at room-temperature, $C = 7.37 \cdot 10^{-4}$ mol·L^{-1}: a) full spectrum, b) zoom on d-d transition.

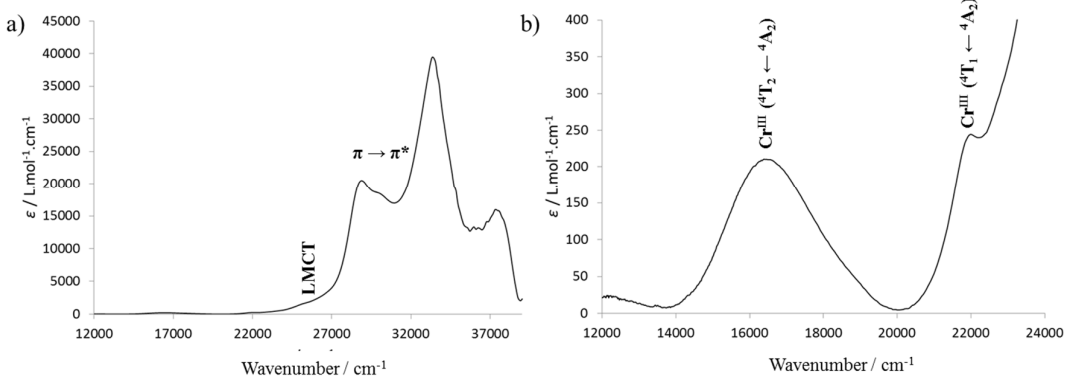

Fig. A1.5 Absorption spectrum of the bimetalic Cr_2Cl_6(bbt) complex in NMP at room-temperature, $C = 6.56 \cdot 10^{-5}$ mol·L^{-1}: a) full spectrum, b) zoom on d-d transition.

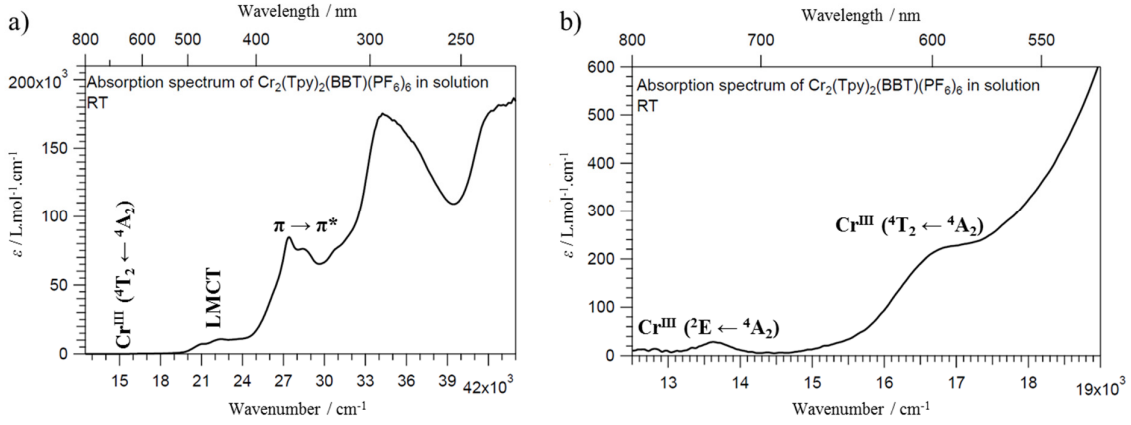

Fig. A1-6 Absorption spectrum of the bimetalic $[Cr_2(tpy)_2(bbt)](PF_6)_6$ complex in ACN at room-temperature, $C = 2.5 \cdot 10^{-5}$ mol·L^{-1}: a) full spectrum, b) zoom on d-d transitions.

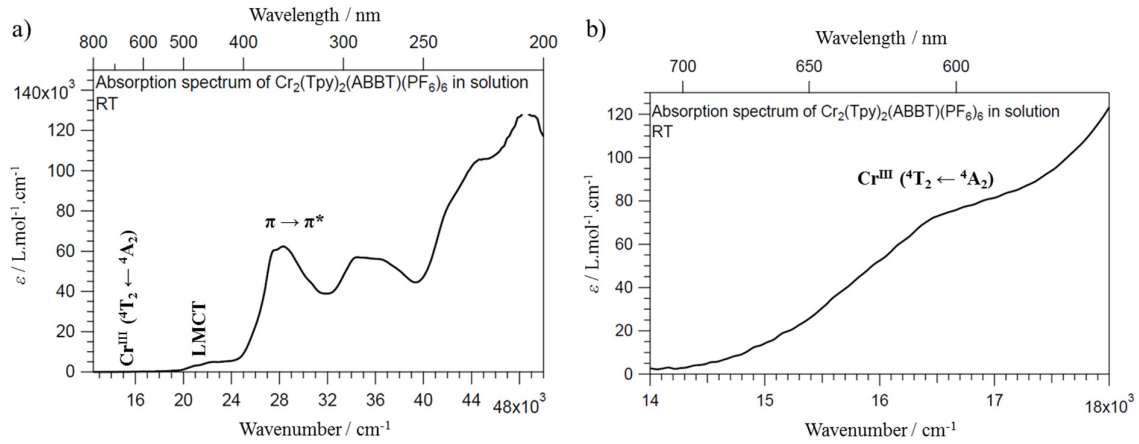

Fig. A1-7 Absorption spectrum of the bimetalic $[Cr_2(tpy)_2(ebbt)](PF_6)_6$ complex in ACN at room-temperature, $C = 6.5 \cdot 10^{-5}$ mol·L^{-1}: a) full spectrum, b) zoom on d-d transitions.

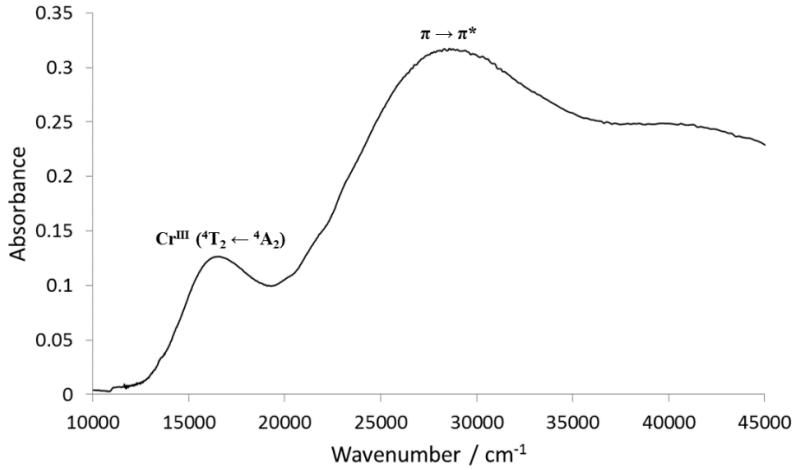

Fig. A1-8 Absorption spectrum of the bimetalic $[Cr_2Cl_6(ebbt)]$ complex diluted in MgO (10%mass of complex) at room-temperature, in the solid state.

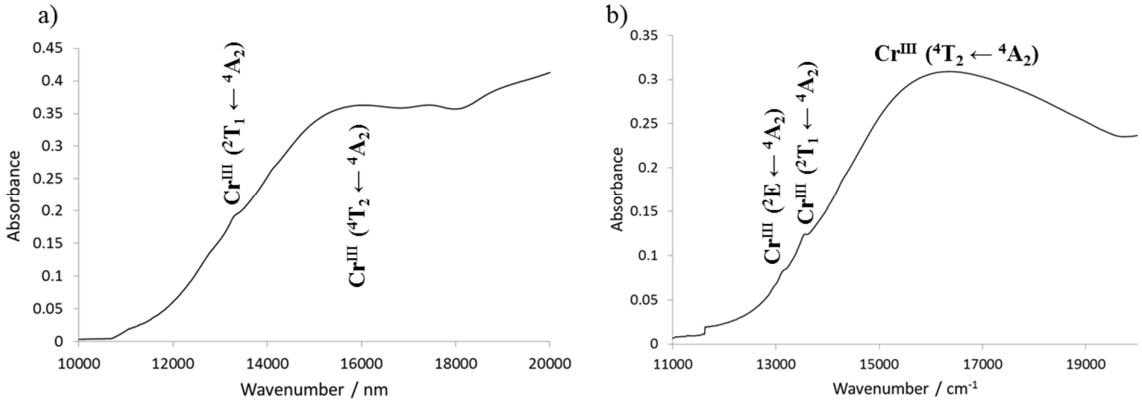

Fig. A1-9 Absorption spectrum at room-temperature, in the solid state, of the dinuclear a) $[Cr_2Cl_6(tppz)]$ complex, and b) $[Cr_2Cl_6(bbt)]$ complex.

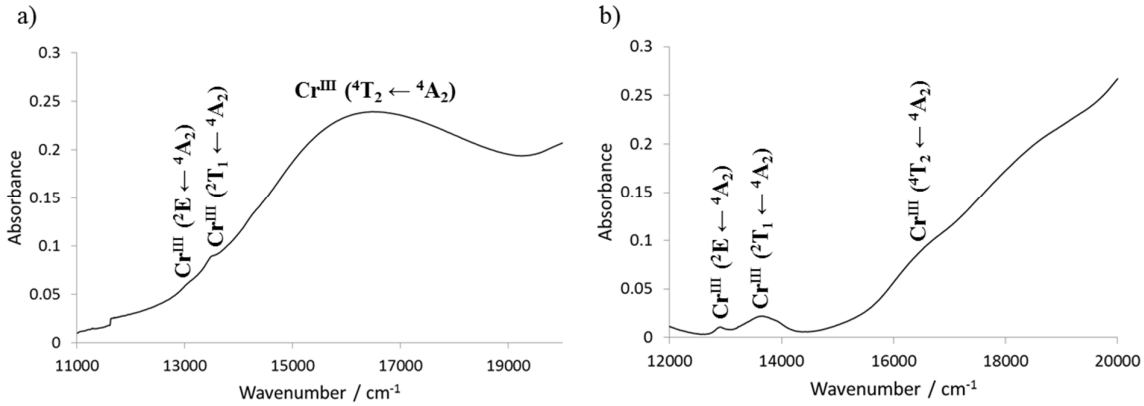

Fig. A1-10 Absorption spectrum at room-temperature, in the solid state, of the dinuclear a) $[Cr_2Cl_6(ebbt)]$ complex, and b) $[Cr_2(tpy)_2(bbt)](PF_6)_6$ complex.

Appendix 2: Emission data

Table A2-1. Phosphorescence $Cr^{III}(^2E)$ emission energy, excited state lifetime ($\tau_{Cr}^{^2E\rightarrow{}^4A_2}$) and associated rate constants ($k_{Cr}^{^2E\rightarrow{}^4A_2} = \left(\tau_{Cr}^{^2E\rightarrow{}^4A_2}\right)^{-1}$) measured for Cr^{III} mononuclear complexes in the solid state (normal font) and frozen solutions (italic font).

Compound	$E(Cr^{III}, {}^2E\rightarrow{}^4A_2)$ /cm^{-1}	T /K	$\tau_{Cr}^{^2E\rightarrow{}^4A_2}$ /ms	$k_{Cr}^{^2E\rightarrow{}^4A_2}$ ($\times10^3$) /s^{-1}
[Cr(tpy)Cl$_3$]	13175	3 K	0.847(10)	1.18(1)
		10 K	0.692(10)	1.45(3)
[Cr(ebzpy)Cl$_3$]	13228	3 K	1.371(10)	73(1)
		10 K	0.267(20)	3.74(9)
[Cr(tppz)Cl$_3$]	13089	3 K	0.242(50)	4.13(31)
		10 K	0.187(50)	5.34(75)
[Cr(tpy)$_2$](PF$_6$)$_3$	12953	3 K	0.560(10)	1.79(4)
		3 K	*0.457(20)*	*2.19(1)*
		10 K	0.372(10)	2.69(4)
		10 K	*0.457(20)*	*2.19(3)*
[Cr(ebzpy)$_2$](PF$_6$)$_3$	13210	3 K	1.242(50)	81(3)
		10 K	0.950(50)	1.05(4)
[Cr(tpy)(ebzpy)](PF$_6$)$_3$	12579	3 K	0.329(20)	3.04(5)
		3 K	*0.265(20)*	*3.77(4)*
		10 K	0.303(20)	3.31(3)
		10 K	*0.264(20)*	*3.78(3)*
[Cr(tpy)(tppz)](CF$_3$SO$_3$)$_3$	12788	3 K	0.342(10)	2.92(6)
		10 K	0.265(10)	3.78(18)

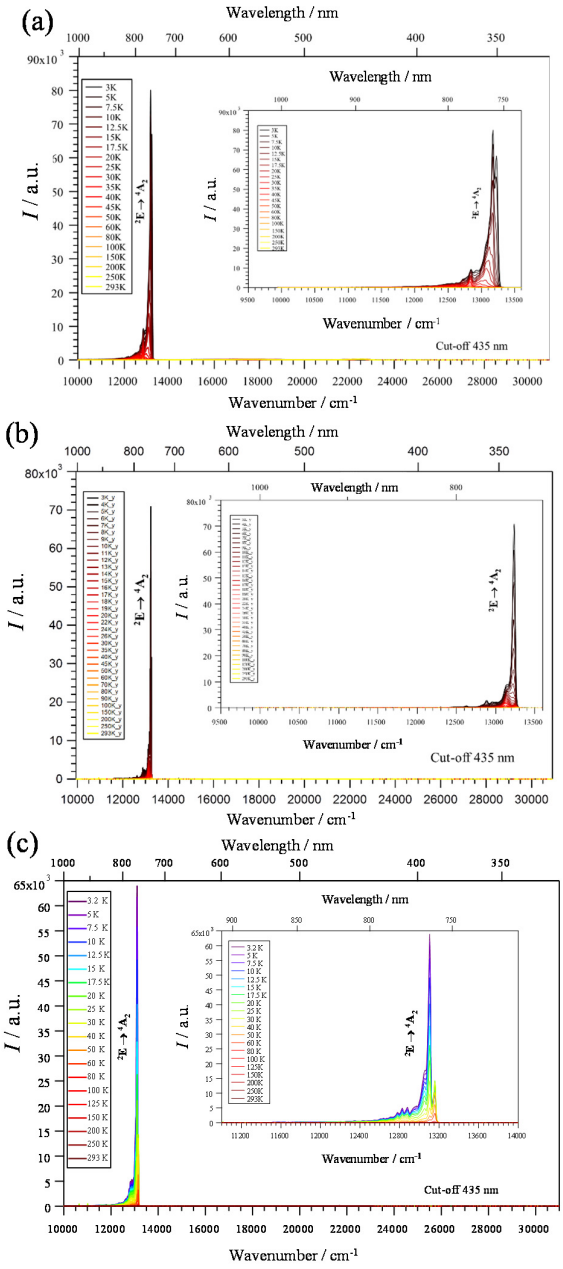

Fig. A2-1 Solid-state emission spectra of mononuclear CrN_3Cl_3 complexes at variable temperature 3-293 K ($\lambda_{exc.}$ = 405 nm, $\bar{\upsilon}_{exc}$ = 24691 cm^{-1}): (a) $[Cr(tpy)Cl_3]$ (integration time = 1000 ms), (b) $[Cr(ebzpy)Cl_3]$ (integration time = 100 ms), ($\lambda_{emis.}$ = 323-1006 nm, $\bar{\upsilon}_{emis.}$ = 30920 - 9935 cm^{-1}, slits aperture = 0.054 mm, xb = 1, 10 accumulations, Laser power (405nm) = 5.4 mW, cutoff 435 nm), and (c) $[Cr(tppz)Cl_3]$, (integration time = 100 ms, $\lambda_{emis.}$ = 321-1004 nm, $\bar{\upsilon}_{emis.}$ = 31160 - 9960 cm^{-1}, slits aperture = 0.05 mm, xb = 1, 5-20 accumulations, Laser power (405nm) = 2.9 mW, cutoff 435 nm).

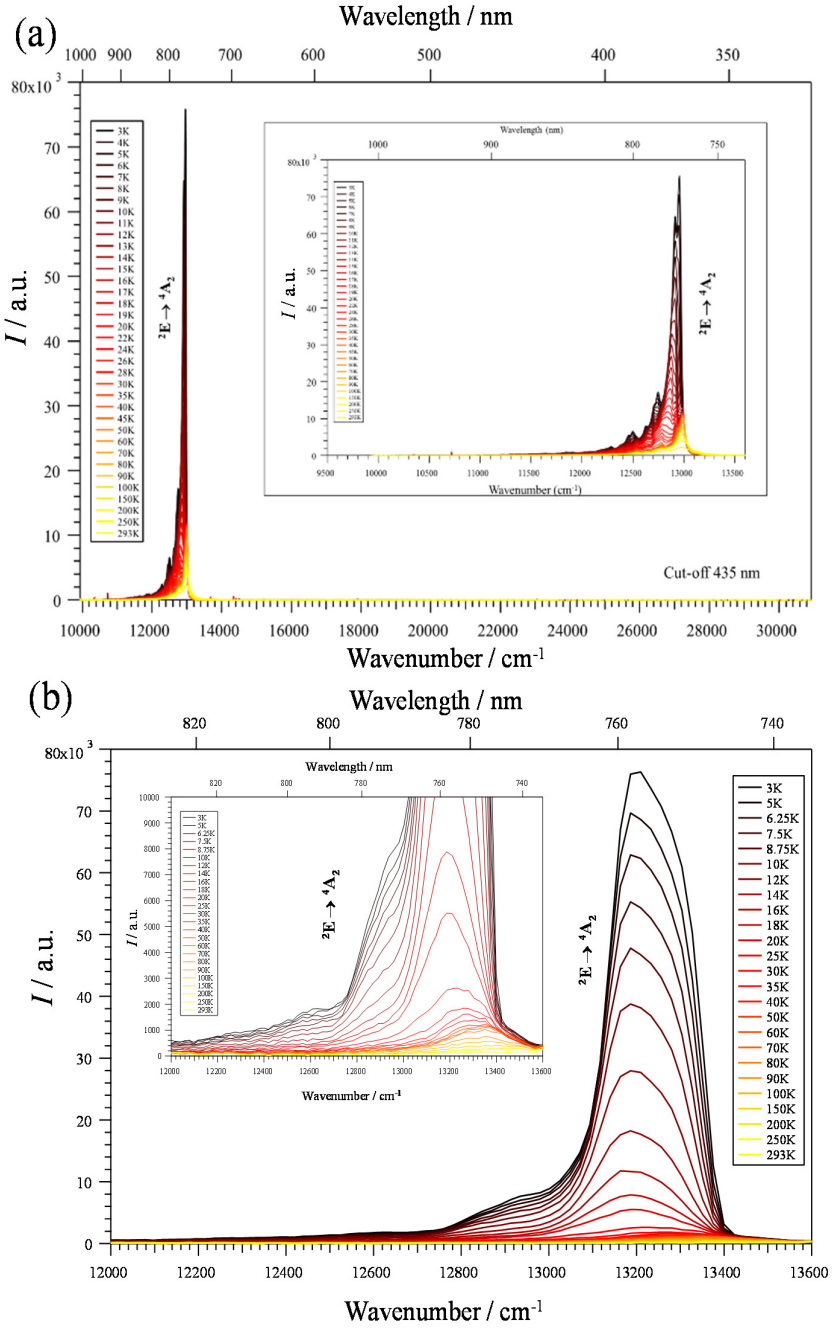

Fig. A2-2 Solid-state emission spectra at variable temperature 3-293 K ($\lambda_{exc.}$ = 405 nm, $\bar{\upsilon}_{exc}$ = 24691 cm^{-1}, $\lambda_{emis.}$ = 323-1006 nm, $\bar{\upsilon}_{emis.}$ = 30920 - 9935 cm^{-1}, Laser power (405nm) = 5.4 mW, cutoff 435 nm), of mononuclear homoleptic chromium complexes (a) $[Cr(tpy)_2](PF_6)_3$ (integration time = 80 ms, slits aperture = 0.054 mm, xb = 1, 10 accumulations) and (b) $[Cr(ebzpy)_2](PF_6)_3$ (integration time = 3000 ms, slits aperture = 0.4 mm, xb = 4, 3 accumulations).

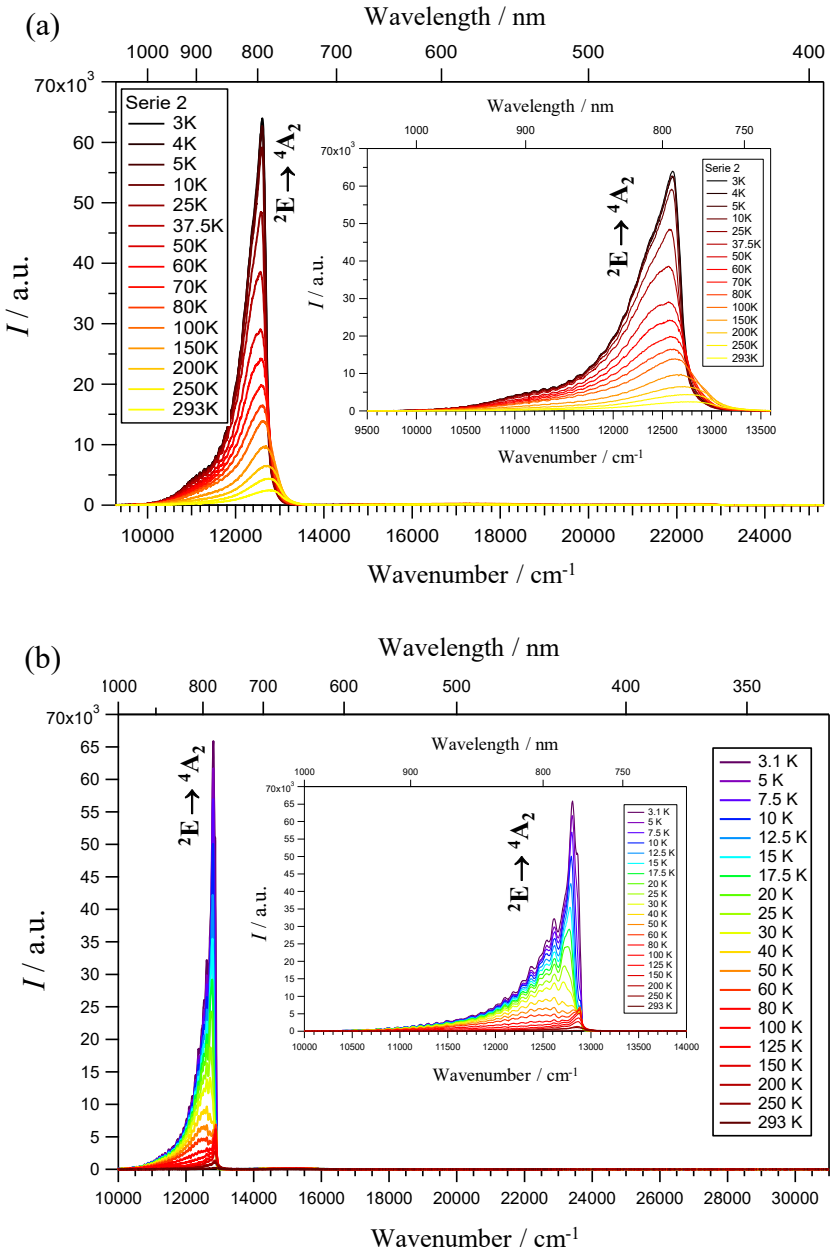

Fig. A2-3 Solid-state emission spectra at variable temperature 3-293 K for ($\lambda_{exc.}$ = 405 nm, $\bar{\upsilon}_{exc}$ = 24691 cm^{-1}) of mononuclear heteroleptic chromium complexes (a) [Cr(tpy)(ebzpy)](PF$_6$)$_3$ (integration time = 150-1200 ms, $\lambda_{emis.}$ = 395-1077 nm, $\bar{\upsilon}_{emis.}$ = 25331 - 9285 cm^{-1}, slits aperture = 0.054-0.2 mm, xb = 1, 10 accumulations, Laser power (405nm) = 5.4 mW, cutoff 435 nm), and (b) [Cr(tpy)(tppz)](CF$_3$SO$_3$)$_3$, (integration time = 100 ms, $\lambda_{emis.}$ = 321-1004 nm, $\bar{\upsilon}_{emis.}$ = 31160 - 9960 cm-1, slits aperture = 0.05 mm, xb = 1, 5-20 accumulations, Laser power (405nm) = 0.6 mW, cutoff 435 nm).

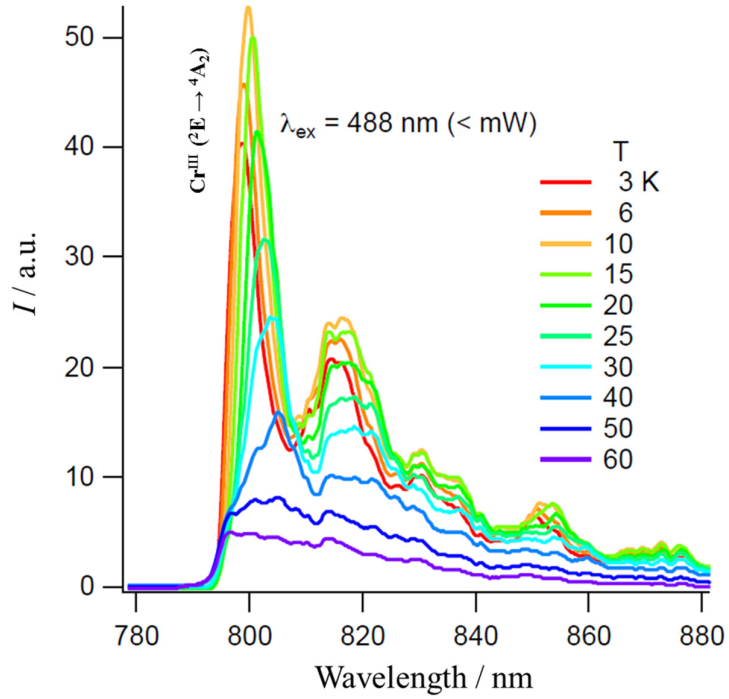

Fig. A2-4 Solid-state emission spectra of dinuclear chromium complex Cr_2Cl_6(tppz) at variable temperature 3-60 K for $\lambda_{exc.}$ = 488 nm, $\bar{\upsilon}_{exc}$ = 20492 cm^{-1}.

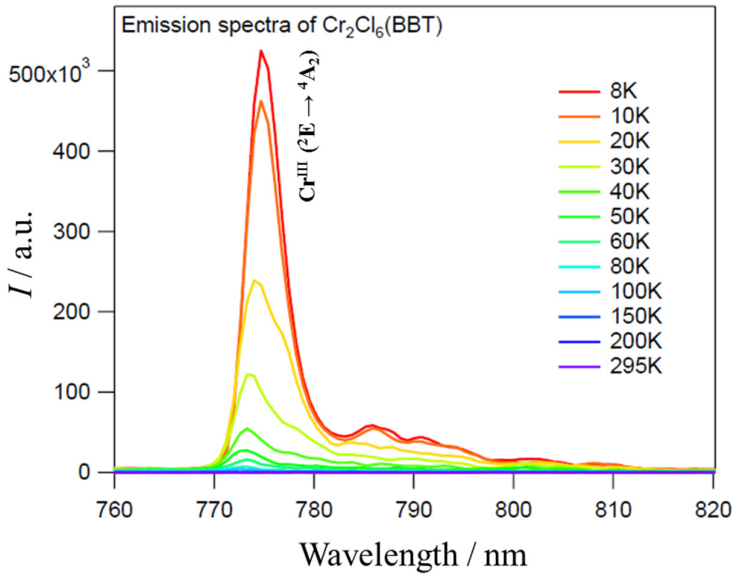

Fig. A2-5 Solid-state emission spectra of dinuclear chromium complex [Cr_2Cl_6(bbt)] at variable temperature 8-295 K for $\lambda_{exc.}$ = 400 nm, integration time = 3000 ms, slits(exc) = 2nm, slits(em) = 1.4 nm, step = 0.7 nm, cutoff 409 nm.

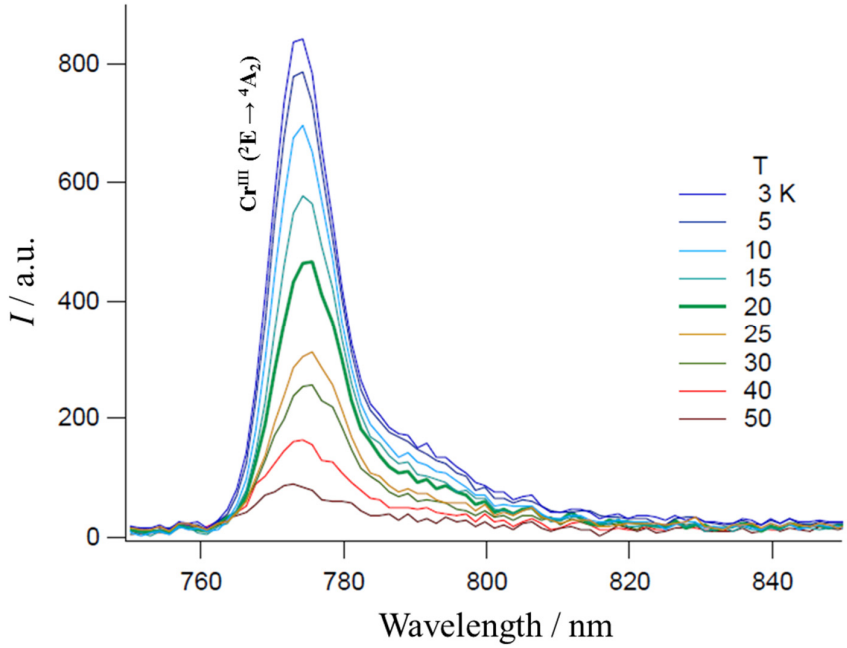

Fig. A2-6 Solid-state emission spectra of dinuclear chromium complex $[Cr_2Cl_6(ebbt)]$ at variable temperature 3-50 K for $\lambda_{exc.}$ = 355 nm, $\bar{\upsilon}_{exc}$ = 28169 cm^{-1}.

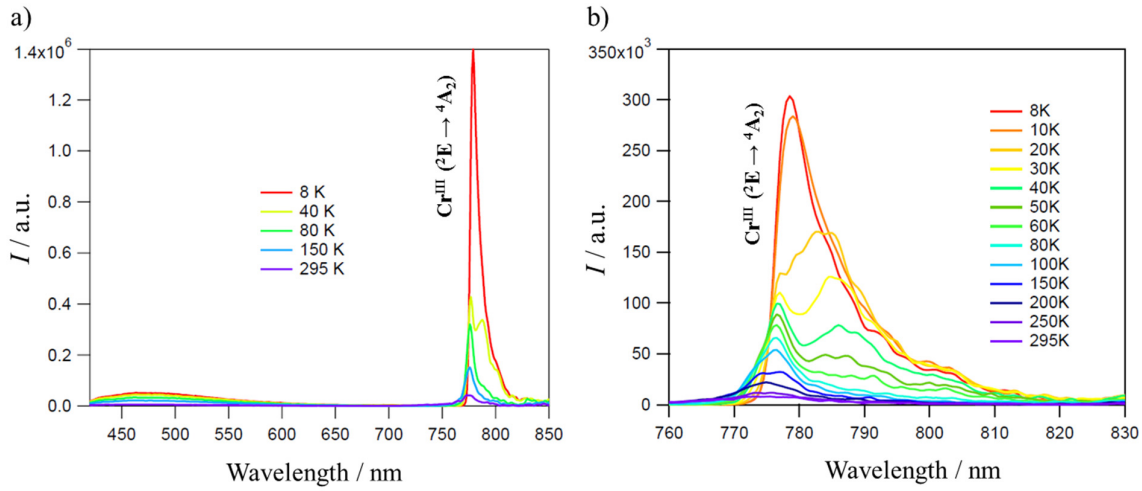

Fig. A2-7 Solid-state emission spectra of dinuclear chromium complex $[Cr_2(tpy)_2(bbt)](PF_6)_6$ at variable temperature 8-295 K for a) λ_{em} = 420-860 nm : $\lambda_{exc.}$ = 400 nm, $\bar{\upsilon}_{exc}$ = 25000 cm^{-1}, integration time = 1000 ms, slits(exc) = 2 nm, slits(em) = 2 nm, step = 1, cutoff 409 nm; b) λ_{em} = 760-830 nm : $\lambda_{exc.}$ = 400 nm, $\bar{\upsilon}_{exc}$ = 25000 cm^{-1}, integration time = 3000 ms, slits(exc) = 2 nm, slits(em) = 1 nm, step = 0.5, cutoff 409 nm.

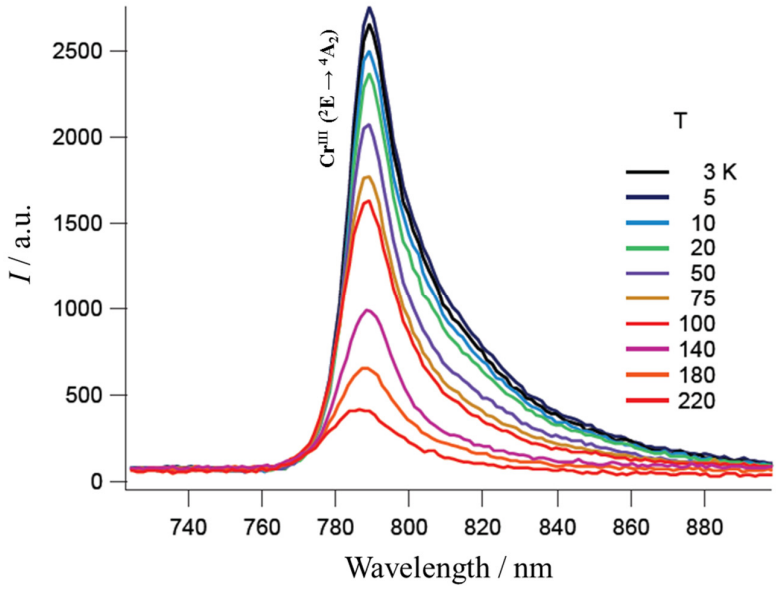

Fig. A2-8 Solid-state emission spectra of dinuclear chromium complex $[Cr_2(tpy)_2(bbt)](PF_6)_6$ at variable temperature 3-220 K for $\lambda_{exc.}$ = 355 nm, $\bar{\upsilon}_{exc}$ = 28169 cm^{-1}.

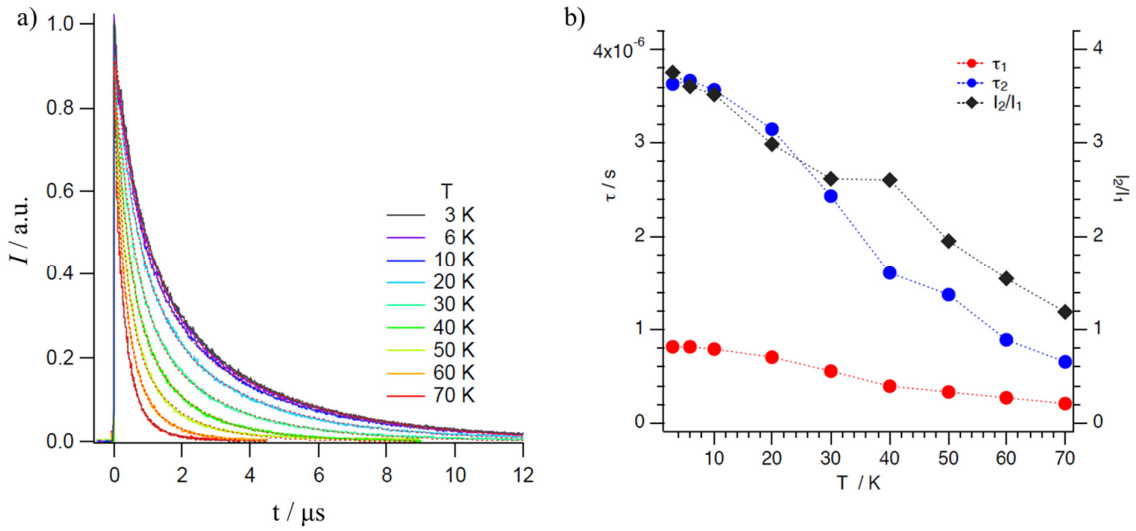

Fig. A2-9 a) Normalised luminescence decay curves for $[Cr_2Cl_6(tppz)]$ at variable temperatures ($\lambda_{exc.}$ = 488 nm, < mW), (---) biexponential fits. b) The two time constants τ_1 and τ_2 and the ratio of corresponding intensities I_2/I_1 for $[Cr_2Cl_6(tppz)]$ as a function of temperature

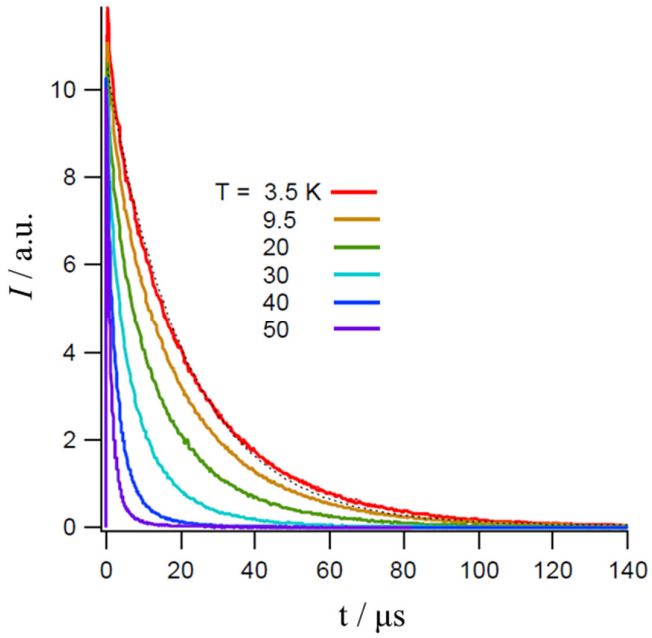

Fig. A2-10 Luminescence decay curves for $[Cr_2Cl_6(bbt)]$ at variable temperatures ($\lambda_{exc.}$ = 488 nm, $\lambda_{detection}$ = 782 ± 5 nm), (---) exponential fit to the decay curve at 3.5 K.

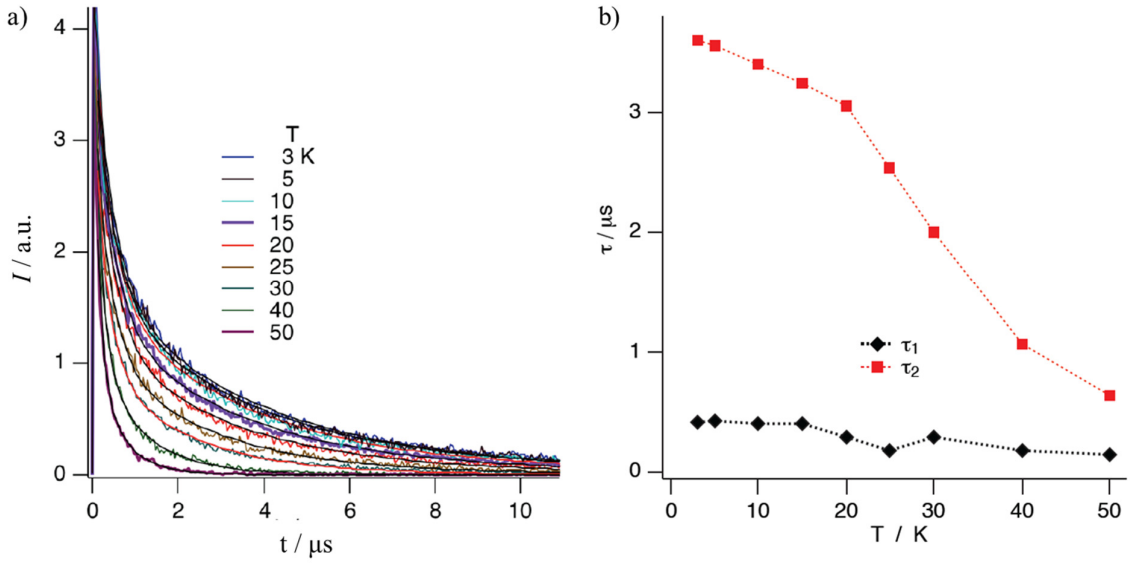

Fig. A2-11 a) Luminescence decay curves for $[Cr_2Cl_6(ebbt)]$ ($\lambda_{exc.}$ = 355 nm, $\lambda_{detection}$ = 760 nm),. Full black lines: double exponential least squares fits. b) Lifetimes of $[Cr_2Cl_6(ebbt)]$ as a function of temperature obtained from a double exponential least squares fit to experimental decay curves. The ratio of the integrated intensities of the fast to the slow decay is approximately 1:10 at all temperatures.

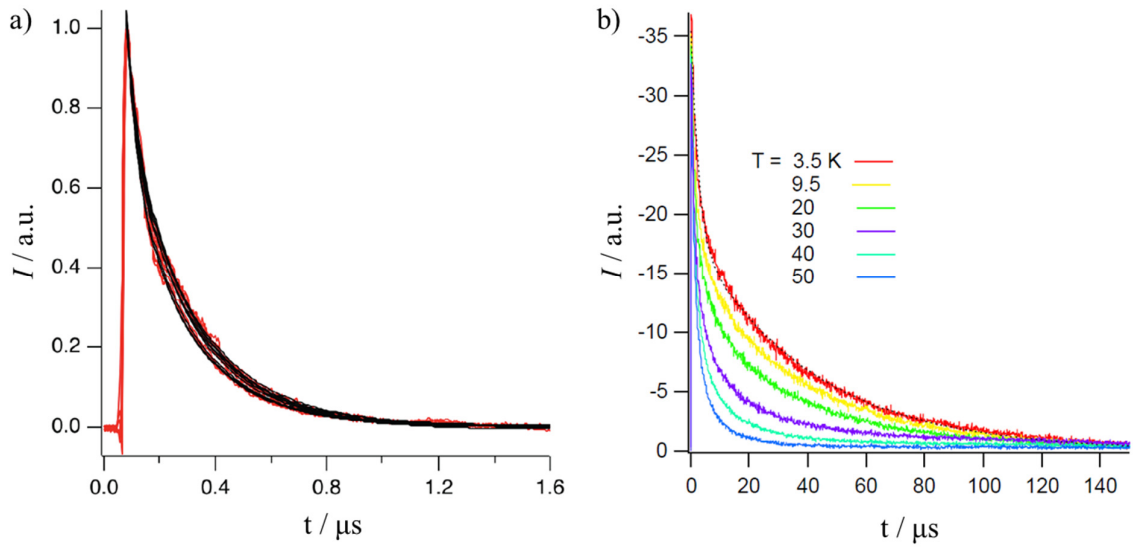

Fig. A2-12 a) Luminescence decay curves of $[Cr_2(tpy)_2(ebbt)](PF_6)_6$ at variable temperatures between 5 and 200 K ($\lambda_{exc.}$ = 355 nm). Black lines: double exponential least squares fits. b) Luminescence decay curves for $[Cr_2(tpy)_2(bbt)](SO_3CF_3)_6$ at variable temperatures from 3.5 to 50 K ($\lambda_{exc.}$ = 488 nm, $\lambda_{detection}$ = 782 ± 5 nm),., (---) biexponential fit at 3.5 K.

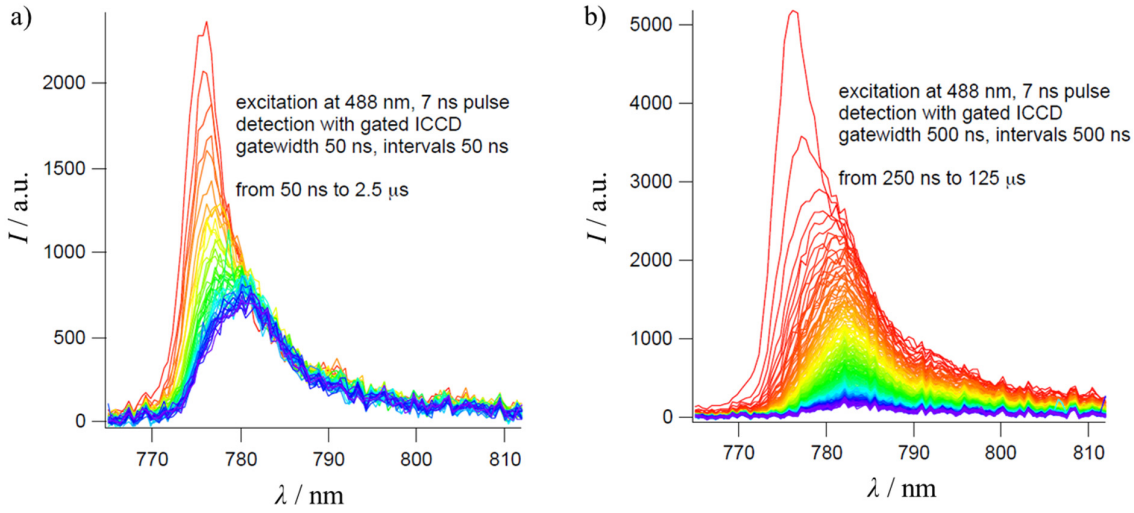

Fig. A2-13 Time-resolved luminescence spectra of $[Cr_2(tpy)_2(bbt)](SO_3CF_3)_6$ at T = 3 K upon pulsed excitation at 488 nm a) recorded with time intervals of 50 ns and b) of 500 ns. In either case the first spectrum is to be regarded as the integrated spectrum during the first interval.

Appendix 3: Statistical factors for thermodynamic equilibria (17)-(20)

According to Benson,[134] the equilibrium constant β in a generic equilibrium is the product of an intrinsic or "chemical" constant K_{chem} and a statistical factor K_σ (eqn A3-1), the latter being estimated by the ratio between the symmetry numbers of the reactant and product species contributing to the equilibrium (eq. A3-2).

$$a\mathrm{A} + b\mathrm{B} \rightarrow c\mathrm{C} + d\mathrm{D} \qquad \beta = K_\sigma \cdot K_{\mathrm{chem.}} \tag{A3-1}$$

$$K_\sigma = \omega_{\mathrm{pm,pn}}^{\mathrm{Ln,L}} = \frac{\prod_i \left(\sigma_{\mathrm{reactancts}}\right)^i}{\prod_j \left(\sigma_{\mathrm{products}}\right)^j} = \frac{\left(\sigma_\mathrm{A}\right)^a \cdot \left(\sigma_\mathrm{B}\right)^b}{\left(\sigma_\mathrm{C}\right)^c \cdot \left(\sigma_\mathrm{D}\right)^d} \tag{A3-2}$$

Determination of the statistical factors for the [ErL] complexes:

$$\mathrm{tppz} + \mathrm{Er(CH_3CN)_9} \xrightarrow{\beta_{1,1}^{\mathrm{Er,\,tppz}}} \left[\left(\mathrm{tppz}\right)\mathrm{Er(CH_3CN)_6}\right] + \ 3\,\mathrm{CH_3CN}$$

Point group	D_{2h}	D_{3h}	C_{2v}	C_{3v}
σ^{ext}	4	6	2	3
σ^{int}	1	3^9	3^6	1
σ^{chir}	1	1	1	1
$\sigma^{tot.}$	2^2	6×3^9	2×3^6	3

$$\mathrm{bbt} + \mathrm{Er(CH_3CN)_9} \xrightarrow{\beta_{1,1}^{\mathrm{Ln,\,bbt}}} \left[\left(\mathrm{bbt}\right)\mathrm{Er(CH_3CN)_6}\right] + \ 3\,\mathrm{CH_3CN}$$

Point group	D_{2h}	D_{3h}	C_{2v}	C_{3v}
σ^{ext}	4	6	2	3
σ^{int}	2	3^9	$2\cdot3^6$	1
σ^{chir}	1	1	1	1
$\sigma^{tot.}$	2^3	6×3^9	$2^2\times3^6$	3

Both [ErL] complexes display the same statistical factor: $\omega_{1,1}^{\mathrm{Er,L}} = \dfrac{\sigma_\mathrm{L} \cdot \sigma_{\mathrm{Er(CH_3CN)_9}}}{\sigma_{\mathrm{Er(L)(CH_3CN)_6}} \cdot \left(\sigma_{\mathrm{CH_3CN}}\right)^3} = 12$

According to the site binding model,[133] the stability constant $\beta_{1,1}^{\mathrm{Er,L}}$ is simply expressed with $f_{\mathrm{N_3,L}}^{\mathrm{Er}}$, which stands for the intrinsic affinity between Er^{3+} and the entering ligand including solvation processes.

$$\beta_{1,1}^{\mathrm{Er,L}} = \omega_{1,1}^{\mathrm{Er,L}} f_{\mathrm{N_3,L}}^{\mathrm{Er}} = 12\, f_{\mathrm{N_3,L}}^{\mathrm{Er}} \tag{17}$$

Determination of the statistical factors for the [ErL$_2$] complexes:

$$2\ \text{tppz} + \text{Er(CH}_3\text{CN)}_9 \xrightarrow{\beta_{1,2}^{\text{Er, tppz}}} \left[\text{Er}\left(\text{tppz}\right)_2 \left(\text{CH}_3\text{CN}\right)_3\right] + 6\ \text{CH}_3\text{CN}$$

Point group	D_{2h}	D_{3h}	C_{2v}	C_{3v}
σ^{ext}	4	6	2	3
σ^{int}	1	3^9	3^3	1
σ^{chir}	1	1	1	1
$\sigma^{tot.}$	4	6×3^9	2×3^3	3

$$2\ \text{bbt} + \text{Er(CH}_3\text{CN)}_9 \xrightarrow{\beta_{1,2}^{\text{Er, bbt}}} \left[\text{Er}\left(\text{bbt}\right)_2 \left(\text{CH}_3\text{CN}\right)_3\right] + 6\ \text{CH}_3\text{CN}$$

Point group	D_{2h}	D_{3h}	C_{2v}	C_{3v}
σ^{ext}	4	6	2	3
σ^{int}	2	3^9	$2^2\cdot3^3$	1
σ^{chir}	1	1	1	1
$\sigma^{tot.}$	2^3	6×3^9	$2^3\times3^3$	3

Both [ErL$_2$] complexes display the same statistical factor: $\omega_{1,2}^{\text{Er,L}} = \dfrac{\left(\sigma_{\text{L}}\right)^2 \cdot \sigma_{\text{Er(CH}_3\text{CN)}_9}}{\sigma_{\text{Er(L)}_2\text{(CH}_3\text{CN)}_3} \cdot \left(\sigma_{\text{CH}_3\text{CN}}\right)^6} = 48$

According to the site binding model,[133] the stability constant $\beta_{1,2}^{\text{Er,L}}$ is expressed by twice $f_{\text{N}_3,\text{L}}^{\text{Er}}$ (the intrinsic affinity interaction between Er^{3+} and ligand including solvation processes) and once $u_{\text{Er}}^{\text{L,L}}$, which represents the microscopic ligand-ligand interaction modifying the intrinsic affinity upon successive ligand binding to a single metallic centre.

$$\beta_{1,2}^{\text{Er,L}} = \omega_{1,2}^{\text{Er,L}} \left(f_{\text{N}_3,\text{L}}^{\text{Er}}\right)^2 u_{\text{Er}}^{\text{L,L}} = 48\left(f_{\text{N}_3,\text{L}}^{\text{Er}}\right)^2 u_{\text{Er}}^{\text{L,L}} \qquad (18)$$

Determination of the statistical factor for the [ErL3] complexes:

$$3\ \text{tppz} + \text{Er(CH}_3\text{CN)}_9 \xrightarrow{\beta_{1,3}^{\text{Er, tppz}}} \left[\text{Er}\left(\text{tppz}\right)_3\right] + \ 9\ \text{CH}_3\text{CN}$$

Point group	D_{2h}	D_{3h}	D_3	C_{3v}
σ^{ext}	4	6	6	3
σ^{int}	1	3^9	1	1
σ^{chir}	1	1	1/2	1
$\sigma^{tot.}$	2^2	6×3^9	3	3

$$3\ \text{bbt} + \text{Er(CH}_3\text{CN)}_9 \xrightarrow{\beta_{1,3}^{\text{Ln,bbt}}} \left[\text{Er}\left(\text{bbt}\right)_3\right] + \ 9\ \text{CH}_3\text{CN}$$

Point group	D_{2h}	D_{3h}	D_3	C_{3v}
σ^{ext}	4	6	6	3
σ^{int}	2	3^9	2^3	1
σ^{chir}	1	1	1/2	1
$\sigma^{tot.}$	2^3	6×3^9	3×2^3	3

Both [ErL3] complexes display the same statistical factor $\omega_{1,3}^{\text{Er,L}} = \dfrac{\left(\sigma_{\text{L}}\right)^3 \cdot \sigma_{\text{Er(CH}_3\text{CN)}_9}}{\sigma_{\text{Er(L)}_3} \cdot \left(\sigma_{\text{CH}_3\text{CN}}\right)^9} = 128$.

According to the site binding model,[133] the stability constant $\beta_{1,3}^{\text{Er,L}}$ is expressed by thrice $f_{\text{N}_3,\text{L}}^{\text{Er}}$ (the intrinsic affinity interaction between Er^{3+} and ligand including solvation processes) and thrice $u_{\text{Er}}^{\text{L,L}}$, which represents the microscopic ligand-ligand interaction modifying the intrinsic affinity upon successive ligand binding to a single metallic centre.

$$\beta_{1,3}^{\text{Er,L}} = \omega_{1,3}^{\text{Er,L}} \left(f_{\text{N}_3,\text{L}}^{\text{Er}}\right)^3 \left(u_{\text{Er}}^{\text{L,L}}\right)^3 = 128\left(f_{\text{N}_3,\text{L}}^{\text{Er}}\right)^3 \left(u_{\text{Er}}^{\text{L,L}}\right)^3 \qquad (19)$$

Determination of the statistical factor for the [Er_2L] complexes:

$$\text{tppz} + 2\ \text{Er}(\text{CH}_3\text{CN})_9 \xrightarrow{\beta_{2,1}^{\text{Er, tppz}}} \left[\text{Er}_2\left(\text{tppz}\right)\left(\text{CH}_3\text{CN}\right)_{12}\right] + \ 6\ \text{CH}_3\text{CN}$$

Point group	D_{2h}	D_{3h}	D_{2h}	C_{3v}
σ^{ext}	4	6	4	3
σ^{int}	1	3^9	3^{12}	1
σ^{chir}	1	1	1/2	1
$\sigma^{tot.}$	2^2	6×3^9	2×3^{12}	3

$$\text{bbt} + 2\ \text{Er}(\text{CH}_3\text{CN})_9 \xrightarrow{\beta_{2,1}^{\text{Er, bbt}}} \left[\text{Er}_2\left(\text{bbt}\right)\left(\text{CH}_3\text{CN}\right)_{12}\right] + \ 6\ \text{CH}_3\text{CN}$$

Point group	D_{2h}	D_{3h}	D_{2h}	C_{3v}
σ^{ext}	4	6	4	3
σ^{int}	2	3^9	$2\cdot3^{12}$	1
σ^{chir}	1	1	1/2	1
$\sigma^{tot.}$	2^3	6×3^9	4×3^{12}	3

Both [Er_2L] complexes display the same statistical factor $\omega_{2,1}^{\text{Er,L}} = \dfrac{\sigma_{\text{L}} \cdot \left(\sigma_{\text{Er(CH}_3\text{CN)}_9}\right)^2}{\sigma_{\text{Er}_2\text{(L)}} \cdot \left(\sigma_{\text{CH}_3\text{CN}}\right)^6} = 72$.

According to the site binding model,[133] the stability constant $\beta_{2,1}^{\text{Er,L}}$ is expressed by twice $f_{\text{N}_3,\text{L}}^{\text{Er}}$ (the intrinsic affinity interaction between Er^{3+} and ligand including solvation processes) and once $u_{\text{L}}^{\text{Er,Er}}$, which represents the microscopic erbium-erbium interaction modifying the intrinsic affinity upon successive metal binding to a single bridging ligand.

$$\beta_{2,1}^{\text{Er,L}} = \omega_{2,1}^{\text{Er,L}} \left(f_{\text{N}_3,\text{L}}^{\text{Er}}\right)^2 u_{\text{L}}^{\text{Er,Er}} = 72\left(f_{\text{N}_3,\text{L}}^{\text{Er}}\right)^2 u_{\text{L}}^{\text{Er,Er}} \qquad (20)$$

Appendix 4: Synthesis of 4',4''''-(ethynyl)bis(2,2':6',2''-terpyridine) (ebbt).

4',4''''-(Ethynyl)bis(2,2':6',2''-terpyridine) (ebbt) was synthetized from the 4-chloro-2,2':6',2''-terpyridine obtained according to a literature procedure.[139] Aromatic nucleophilic substitution using HI in acetic acid first lead to 4-iodo-2,2':6',2''-terpyridine. Since aryl iodides were known to be activated under smooth condition, a room temperature pallado-catalysed cross coupling Sonogashira reaction yielded the intermediate 4-(trimethylsilyl-ethynyl)-2,2':6',2''-terpyridine, which was futher deprotected using basic conditions to afforde 4-(ethynyl) -2,2':6',2''-terpyridine. The bridging ebbt was finally obtained by a Sonogashira cross coupling between the 4-iodo-2,2':6',2''-terpyridine and 4-(ethynyl) -2,2':6',2''-terpyridine using $Pd(PPh_3)_4$ as catalyst instead of $PdCl_2(PPh_3)_2$ in order to avoid the in situ generation of Pd^0 from Pd^{II} and the formation of Glaser homo coupling products.

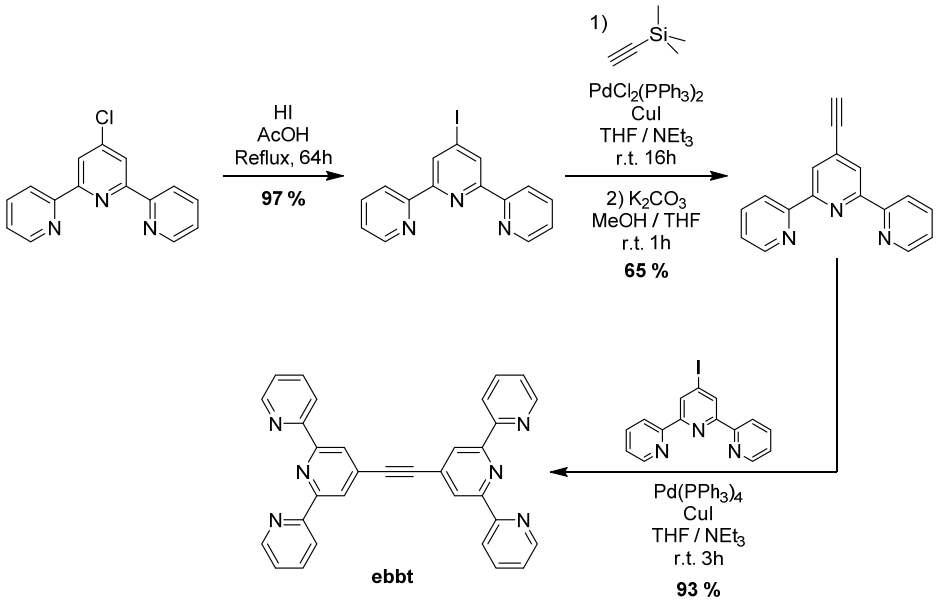

Scheme A4-1. Synthesis of the ebbt bridging ligand

4'-Iodo-2,2':6',2''-terpyridine

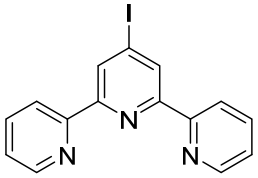

4'-Chloro-2,2':6',2''-terpyridine (1.0 g, 3.74 mmol, 1 eq), glacial acetic acid (10 mL), and HI 57 % in water (10 mL), were introduced in a round bottom flask. After 64 hours refluxing, the mixture was diluted in water, NaOH was added until basic pH. The aqueous layer was extracted by dichloromethane (3 times), and the combined organic layers were washed by water (4 times),

dried over anhydrous $MgSO_4$, and filtered. Solvent evaporation yielded pure 4'-iodo-2,2':6',2"-terpyridine as a white solid (97 %, 1.3 g).

^{1}H NMR: (400 MHz, $CDCl_3$) δ 8.86 (s, 2H), 8.70 (dd, *J* = 4.8Hz, *J* = 0.9 Hz, 2H), 8.57 (d, *J* = 7.9 Hz, 2H), 7.86 (m, 2H), 7.35 (ddd, *J* = 7.5 Hz, *J* = 4.8Hz, *J* = 1.2 Hz, 2H). ^{13}C NMR: (100 MHz, $CDCl_3$) δ 155.7, 154.8, 149.2, 137.3, 130.4, 124.4, 121.6, 107.8. ESI-MS *m/z*: $[M+H]^+$ calc ($C_{15}H_{11}IN_3$): 360.0, found: 360.6.

4'-Ethynyl-2,2':6',2"-terpyridine

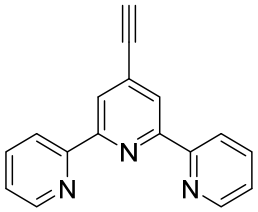

4'-iodo-2,2':6',2"-terpyridine (680 mg, 1.89 mmol, 1 eq), $PdCl_2(PPh_3)_2$ (133 mg, 0.189 mmol, 10 mol%), CuI (72 mg, 0.378 mmol, 20 mol%), and a mixture of NEt_3 / THF (1:2) previously degassed by argon bubbling (30 min) were introduced in a Schlenk tube under argon. Trimethylsilyacetylene (TMSA, 1.6 mL, 11.3 mmol, 6 eq) was then added. The mixture was stirred at room temperature for 16 hours. After solvent evaporation, the crude product was dissolved in dichloromethane and a few drops of tris(2-aminoethyl)amine were added. The organic layer was washed by water (4 times), dried over anhydrous $MgSO_4$, filtered, and the solvent was evaporated. The crude product was purified by column chromatography (Al_2O_3: cyclohexane/dichloromethane (0-100 %) to give 665 mg of 4-(trimethylsilyl-ethynyl) -2,2':6',2"-terpyridine which was introduced in a round bottom flask. K_2CO_3 (184 mg, 1.33 mmol, 2 eq), THF (10 mL), and MeOH (10 mL) were added, and the mixture was stirred at room temperature for 1 hour. Solvent was evaporated, the solid was dissolved in dichloromethane and purified by plug filtration (Al_2O_3: CH_2Cl_2/AcOEt). Solvent evaporation yielded pure 4'-Ethynyl-2,2':6',2"-terpyridine as a white solid (65 %, 319 mg).

^{1}H NMR: (400 MHz, $CDCl_3$) δ 8.71 (d, *J* = 4.7 Hz, 2H), 8.61 (d, *J* = 8.0 Hz, 2H), 8.54 (s, 2H), 7.87 (m, 2H), 7.36 (dd, *J* = 7.6 Hz, *J* = 4.7 Hz, 2H), 3.32 (s, 1H). ^{13}C NMR: (100 MHz, $CDCl_3$) δ 155.6, 155.4, 149.2, 137.3, 132.5, 124.3, 123.7, 121.5, 81.8, 81.6. ESI-MS *m/z*: $[M+H]^+$ calc ($C_{17}H_{12}N_3$): 258.1, found: 258.5.

4',4''''-(ethynyl)bis(2,2':6',2''-terpyridine (ebbt)

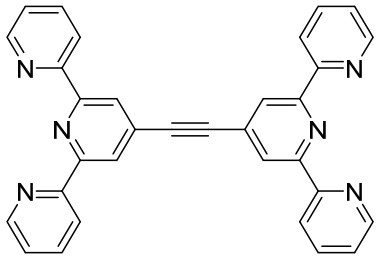

4’-Iodo-2,2’:6’,2”-terpyridine (180 mg, 0.501 mmol, 1 eq), 4’-ethynyl-2,2’:6’,2”-terpyridine (142 mg, 0.551 mmol, 1.1 eq), $Pd(PPh_3)_4$ (58 mg, 0.0501 mmol, 10 mol%), CuI (19 mg, 0.100 mmol, 20 mol%), and a mixture of NEt_3 (8 mL) / THF (12 mL) previously degassed by argon bubbling 1hour, were introduced into a Schlenk tube under argon. After 3 hours stirring at room temperature, a white precipitate appeared, and the mixture was diluted in MeOH and filtered through a plug of Celite. The plug was then eluted with boiling $CHCl_3$, and the collected organic phases were evaporated to give 4',4''''-(ethynyl)bis(2,2':6',2''-terpyridine) (ebbt) as a white solid (93 %, 227 mg).

^{1}H NMR: (400 MHz, $CDCl_3$) δ 8.75 (d, J = 4.2 Hz, 4H), 8.64 (s, 4H), 8.63 (d, J = 7.1 Hz, 4H), 7.89 (m, 4H), 7.37 (ddd, J = 7.5 Hz, J = 4.8Hz, J = 1.2 Hz, 4H). ^{13}C NMR: (100 MHz, $CDCl_3$) δ 155.9, 155.7, 149.4, 137.1, 132.6, 124.2, 123.3, 121.4, 91.4. ESI-MS *m/z*: $[M+H]^+$ calc ($C_{32}H_{21}N_6$): 489.2, found: 489.9.